$\text{AD. } 1982$

ornl

**OAK
RIDGE
NATIONAL
LABORATORY**

UNION
CARBIDE

MASTER

Evaluation of Neutron and Gamma-Ray-Production Cross Sections for Natural Iron (ENDF/B-V MAT 1326)

C. Y. Fu
F. G. Perey

OPERATED BY
UNION CARBIDE CORPORATION
FOR THE UNITED STATES
DEPARTMENT OF ENERGY

Contract No. W-7405-eng-26

Engineering Physics Division

EVALUATION OF NEUTRON AND GAMMA-RAY-PRODUCTION CROSS SECTIONS

FOR NATURAL IRON (ENDF/B-V MAT 1326)

C. Y. Fu and F. G. Perey

Date Published - November 1980

OAK RIDGE NATIONAL LABORATORY
Oak Ridge, Tennessee 37830
operated by
UNION CARBIDE CORPORATION
for the
DEPARTMENT OF ENERGY

TABLE OF CONTENTS

ABSTRACT

This document deals with the evaluation of neutron and gamma-ray-production cross sections for natural iron. Improvements for ENDF/B-V MAT 1326 are described and graphically compared with the previous version. A summary of the previous version and a general description of the current status of the evaluation are also given.

I. INTRODUCTION

This document deals with the evaluation of neutron and gamma-ray-production cross sections for natural iron for ENDF/B. Revisions of ENDF/B-IV MAT 1192 for ENDF/B-V MAT 1326 are described in Section II. Graphical comparisons of Version V with Version IV are shown where necessary.

Because no detailed documentation has been provided for ENDF/B-IV, we give in Section III a summary of the ENDF/B-IV work to bridge the gap between Version III[1] and Version V. This gap is small, however, since part of the work done for Version IV was revised again in Version V and part of the calculations have been documented.[2]

A general description of ENDF/B-V MAT 1326 as it now stands is given in Section IV.

II. REVISIONS FOR ENDF/B-V

The following changes were made to go from ENDF/B-IV to ENDF/B-V.

Resonance Parameters

Resonance parameters for ^{54}Fe, ^{56}Fe, and ^{57}Fe were taken from a comprehensive evaluation of these parameters by Perey and Perey.[3] For ^{58}Fe, the resonance parameters were taken from the proposed ENDF/B-V ^{58}Fe(n,γ) dosimetry file.[4] The resonance range was extended from 60 keV in ENDF/B-IV to 400 keV in ENDF/B-V. The number of resonances was increased from 29 to 312.

The primary purpose of extending the resonance range was to give a detailed description of the capture cross sections between 60 keV and 400 keV, an important range for fast breeder analysis.

Through the resonance parameters, many narrow p- and d-wave resonances, seen only in capture measurements, were introduced to the total cross sections.

The format restriction of using a single constant scattering radius resulted in some problems in generating the background cross sections, as discussed below.

Total Cross Sections

The File-3 Section-1 data in the resolved resonance range from 155 eV to 400 keV are background cross sections and were chosen to reproduce the broad s-wave structures in the ENDF/B-IV evaluation. Narrower s-waves and higher partial waves were left as defined by the parameters without any background corrections. The energies, peak cross sections and areas of the latter resonances are thought to be better defined now because of additional input to the evaluation of the resonance parameters from high-resolution capture and elastic-scattering data. Comparisons of ENDF/B-V with IV are displayed in Figs. 1-4. The background cross sections as entered in File 3 Section 1 are large and become mostly negative above 200 keV. The effective scattering radius used is 0.5×10^{-12} cm for all isotopes. We have tried smaller and larger radii, none of which gave better results. A radius of 0.65×10^{-12} cm yielded a good fit to the total cross sections below 50 keV, while 0.4×10^{-12} cm gave good results from 300 to 400 keV. So it appears that an energy-dependent effective scattering radius would help. But such a radius is presently not allowed.

We have studied the integral test by Maerker et $al.$[5] and the pseudo-integral test by Smith et $al.$[6] for the total cross sections of Fe from 1 to 5 MeV. Maerker et $al.$ indicate that the total cross sections of Fe from 1.5 to 2.4 MeV are 4% too low, while Smith et $al.$ say that they are 5% too high. This may not be a contradiction however, because the deep penetration (8 to 19 inches) measurement of Maerker et $al.$ is sensitive to the cross-section minima while the broad-resolution thir-sample measurement of Smith et $al.$ is not. It is therefore probable that the total cross-section maxima from 1.5 to 2.4 MeV are not sharp enough and the minima are not deep enough. There are deficiencies in other energy ranges too and all seem complicated. We did not attempt to resolve this problem for ENDF/B-V but are recording the above as a reminder for future measurements and/or evaluations.

Elastic Scattering Cross Sections

In the new resonance range from 155 eV to 400 keV the capture cross sections are small so the elastic cross sections are nearly the same as

the total cross sections. Due to decreases in the inelastic scattering cross sections described below, the elastic scattering cross sections from 846 keV to 1.3 MeV were correspondingly increased.

Inelastic Scattering to the 846-keV Level

Kinney and Perey[7] have reported high-resolution data for neutron inelastic scattering to the 846-keV level from threshold to 2.1 MeV by measuring the pertinent gamma rays at 30, 90, and 125 degrees. The data at these three angles allow the determination of the a_2 and a_4 Legendre coefficients for the angular distribution of the outgoing gamma rays, and therefore the determination of the integrated cross sections. The 125-degree data agree well with a similar measurement by Voss et al.[8] at the same angle which was adopted as the integrated cross sections for ENDF/B-IV. However, the new integrated cross sections up to 1.3 MeV are about 20% smaller. Smoothed results of the high-resolution data also agree well with other available data, including those of A. B. Smith[9] and D. L. Smith,[10] as shown in detail in ref. 7. We therefore adopted the high-resolution data for ENDF/B-V from threshold to 1.3 MeV. Figure 5 is reproduced from Fig. 6 of ref. 7.

Other Neutron-Emission Reactions

The Monte Carlo analysis[11] (using ENDF/B-IV) of a recent integral measurement[12] of the secondary neutron spectra with a white source (ORELA) (concludes that the inelastic scattering cross sections of a few low-lying discrete levels rise too fast just above threshold, that some of the discrete inelastic scattering cross sections die off too rapidly with energy, and that the (n,2n) cross sections are too large from threshold (11.4 MeV) to 12.5 MeV. The first point is difficult to resolve for we have good model fit to the available data. The second point can probably be resolved by a model calculation with pre-compound effects (ENDF/B-IV already has direct-reaction cross sections in 15 of the 26 discrete levels). The third point is contradictory to some newly available data discussed in the next paragraph.

No (n,2n) data existed below 14 MeV when we were evaluating for ENDF/B-IV, so calculated cross sections were used. A recent measurement for ^{56}Fe(n,2n) cross sections by Frehaut et al.[13] indicates that our

evaluated (n,2n) cross sections are, contrary to the above, too low from threshold to 13 MeV after correcting for the small contributions from the minor isotopes. The new data show good agreement with the evaluation from 13 to 15 MeV.

Johnson[14] reported calculated and measured neutron leakage spectra from a D-T source in an iron sphere 76 cm in diameter and 30 cm thick. The calculated spectra using ENDF/B-IV from 1 to 12 MeV are factors of 3-4 too low. This indicates that the isotropic assumption taken for ENDF/B-IV for the inelastic scattering to the continuum states is completely inadequate. Although we do have some angular data for 14-MeV incident neutrons, extrapolation to other energies requires elaborate model calculations which we did not have time to do. Such calculations also appear necessary to resolve some of the deficiencies discussed in the above paragraphs.

Capture Cross Sections

The extension of the resonance parameters from 60 to 400 keV has the largest impact on the capture cross sections as shown in Figs. 6-16. The ENDF/B-IV cross sections from 60 keV to 400 keV are smooth varying with energy, missing the broad peaks of several large s-wave resonances. Below 60 keV there are also differences due to changes in the capture areas and several additional resonances. Between 400 keV and 500 keV, the capture cross sections were the same as in ENDF/B-IV.

From 500 to 850 keV, 50-keV averages reported by Allen *et al.*[15] were used. These data were later found to be consistent with those measured by Le Rigoleur *et al.*[16]

Above 2 MeV, the capture cross sections were increased to go through a data point near 14 MeV.[17] Comparison of the capture cross sections from 500 keV to 20 MeV with ENDF/B-IV values is shown in Fig. 17.

Angular Distributions of Secondary Neutrons from Elastic Scattering

High-resolution data on the angular distributions of secondary neutrons scattered elastically were measured by Kinney and Perey[18] from 40 keV to 2.1 MeV. These data are in the form of Legendre coefficients for over 5000 energies. These were thinned to about 400 energy points for entering into the file. The thinning was done with a code obtained

from Young.[19] The Legendre coefficients were converted to angular distributions for thinning to a tolerance of 50% with linear interpolation. Because the angular distributions considered here often fluctuate by one order of magnitude from resonance to resonance, the main features of the original data were retained. The first two coefficients are compared with ENDF/B-IV values in Figs. 18-25.

Gamma-Ray Production Cross Sections

When we were evaluating the gamma-ray production cross sections for ENDF/B-IV, there were two major sets of data available, one by Orphan *et al.*[20] and the other by Dickens *et al.*[21] The integrated cross sections of the two sets diverge above 6 MeV, the Orphan set averaging 1.6 barns larger than the Dickens set from 11 to 15 MeV. Our calculated results are in good agreement with the Orphan set up to 11 MeV but get closer to the Dickens data near 15 MeV. With some hesitation we took for ENDF/B-IV the calculation as the integral gamma-ray production cross section and the Dickens data were normalized to this to provide the energy distributions.

To resolve the above discrepancy, a new measurement was undertaken by Chapman and Morgan[22] using ORELA. The new data agree well with the Orphan data, therefore indicating that the earlier ORELA data taken by Dickens *et al.*[21] have some unknown errors. This also indicates that our calculated cross sections are too low above 11 MeV, a calculational fault which we can overcome now by including the pre-compound cross sections in the gamma-ray cascade calculation. So we feel that the gamma-ray production cross sections and spectra are now well known for incident neutron energies from 0.85 to 20 MeV, and we took the Chapman and Morgan data for ENDF/B-V. Detailed comparisons of these data with others and with ENDF/B-IV are given in ref. 22.

Because we did not re-calculate the neutron cross sections above 11 MeV, the calculated neutron distributions, which we still have in the file, may be somewhat inconsistent with the new gamma-ray distributions. The resulting energy imbalance cannot be easily corrected without a model calculation.

From 0.85 to 2.122 MeV, the 0.864-MeV and the 1.408-MeV gamma rays from inelastic scattering were removed from the Chapman and Morgan data to obtain three energy distributions that are representative of the capture components. Below 0.85 MeV, the original capture gamma-ray evaluation was retained, but the energy distributions were re-structured to fewer points by using variable energy bins.

Covariances for the Resonance Parameters

This file was evaluated and separately reported by Perey and Perey.[3]

Covariances for File 3 Data

Covariance data are given for MF=32, MT=151 and MF=33, MT=1, 2, 3, 4, 16, 22, 28, 51-76, 91, 102-107. Derived sections (NC subsections) reflect exactly the way the cross-section files were generated.

In general, covariances were determined from $\pm 2\sigma$ error bands. The error bands were extended and enlarged to cover energy regions lacking experimental data and then split up to cover different correlation ranges. Long range covariances reflect systematic errors common to all data sets. Medium range covariances reflect differences in energy coverage by different data sets and differences in experimental techniques within the same data sets. Short range covariances reflect meaningful structures in the cross sections and/or threshold effects. Statistical errors are, in principle, nonexistent in the evaluated cross sections.

For all threshold reaction cross sections, covariances have at least two components -- an absolute and a fractional. The absolute component represents with few numbers the usually large variation of uncertainties near threshold and for the high-energy tail. The fractional component picks up the rest of the covariances. For the more important reactions, such as MT=51, two absolute and two fractional components were used.

A constant uncertainty of 50 mb was used to represent the total cross section minima. This corresponds to about 12% for the 24-keV minimum.

Independent evaluations and error estimates by another party, such as the evaluation for the inelastic scattering cross sections of the 846-keV level by Smith,[23] provided objectivity. Integral measurements and analyses also add objectivity.

III. SUMMARY OF ENDF/B-IV

This version, ENDF/B-IV MAT 1192, superseded the previous version, ENDF/B-III MAT 1180. One of the purposes of this work was to revise the secondary neutron energy distributions from various neutron-producing reactions. New data for the secondary neutron distributions had become available[24,25] and the pulsed-sphere measurements[26] and related calculations[26,27] indicated that the previously evaluated distributions were poor. A reevaluation of the gamma-ray-production cross sections was also called for because newly available data[28] showed large disagreement with the data set[29] upon which the previous evaluation was based. In an attempt to solve these problems an extensive model analysi. ·vas made. A third purpose of this work was to incorporate the multi-sample high-resolution measurements[30] of total cross sections that had just become available. The resulting changes are summarized below.

1. Total cross section between 30 keV and 2 MeV — peaks and valleys were refined based on three sets of ORELA measurements[30] using 2.5-, 10-, and 30-cm samples.

2. Nonelastic — obtained by compromising three pieces of information, namely, the measured nonelastic cross section, the difference between the evaluated total cross section and the available elastic scattering cross section, and the theoretical interpretation of the total gamma-ray-production cross section. The calculated nonelastic cross section was normalized to this result for constraining the subsequent calculations.

3. Inelastic scattering — six more discrete levels were added based on the Hauser-Feshbach[31] and DWBA[32] calculations in order to include the 4.505-MeV collective state as a discrete level. The direct-interaction components were included in 15 of the 26 discrete levels.[33] The direct-interaction component was included in the continuum using an empirical treatment.[34] MT=51 (0.846-MeV level) was changed between 2 and 5 MeV according to an evaluation by Smith[23] which was based on all available data and his recent measurement. MT=52 (the 1.408-MeV level in ^{54}Fe) was revised based on recently available data.[35]

4. The Hauser-Feshbach method was used to calculate the [(n,n')+ (n,nx)], [(n,p)+(n,px)], and [(n,α)+(n,αx)] cross sections. The [(n,n')+ (n,nx)] cross section above 4.531 MeV was split into the (n,n') continuum, (n,2n), (n,np), and (n,nα) cross sections using a statistical-empirical model.[34] The empirical aspects include giant-dipole gamma-ray competition, angular-momentum correction for the second outgoing particle, and direct or preequilibrium emission of the first particle.

5. The (n,p) cross section was well defined by measurements[36,37] and that of ^{56}Fe was well fitted by calculation up to 13 MeV. The (n,pn) cross section was taken to be the difference between the calculated ^{56}Fe [(n,p)+(n,px)] cross section and the measured ^{56}Fe(n,p) cross section. The neutron distribution for the (n,pn) reaction was calculated and was averaged with that of the (n,np) reaction for MT=28.

6. There is no measured ^{56}Fe(n,α) cross section. The calculated ^{56}Fe(n,α) cross section was restrained by the 14-MeV empirical value and the measured fission-spectrum averages. The ^{54}Fe(n,α) cross section was taken from a calculation by Kirouac and Slavik.[38] The (n,αn) cross section and neutron distribution were calculated and were combined with those of the (n,nα) reaction for MT=22.

7. The (n,d), (n,t), and (n,^{3}He) cross sections were based on calculations using the Pearlstein empirical model and parameters.[39]

8. The two major sets[28,29] of gamma-ray-production cross sections agree within experimental errors for incident neutron energies below 6 MeV and then start to diverge, the GRT set[28] averaging 1.6 barns larger than the ORNL set[29] in the 11 to 15 MeV region. Other available data were too limited to resolve this discrepancy. The calculated results are intermediate between the two, being closer to the GRT measurement below 12 MeV and closer to the ORNL data above 12 MeV. We chose the ORNL data for the energy distributions (File 15) as these were given in adequate neutron bins and were the only data available from 15 to 20 MeV. The gamma rays below 0.69 MeV were not measured and were filled in using the calculated values. Up to 10 MeV incident neutron energy the energy conservation law relating the calculated outgoing particle energy and the evaluated gamma-ray energy was applied to determine the gamma-ray multiplicities.

From 10 to 16 MeV the calculated multiplicities were used and were extrapolated to 20 MeV according to the shape given by the ORNL measurement.

IV. GENERAL DESCRIPTION FOR ENDF/B-V

The following description for each file and section is for ENDF/B-V. The references given are only the more important ones. Where a computer code is referred to, it means that interpolation and extrapolation of the given experimental data were based on calculations.

File 2. Resonance Parameters

Multilevel Breit-Wigner parameters are given for all isotopes in the energy range 155 eV to 400 keV.[3,4]

File 3. Neutron Cross Sections

Section 1. Total Interaction

.00001 eV to 330 keV[30,40,41]

330 keV to 20 MeV[30,42-44]

Section 2. Elastic Scattering

Derived by subtracting the non-elastic cross section from the total cross section.

Section 3. Non-Elastic Interaction

See Section III above.

Section 4. Total Inelastic Scattering

Derived by adding inelastic scattering cross sections for exciting discrete levels and the continuum.

Section 16. (n,2n) Reaction

See Section II above and ref. 45.

Section 22. (n,nα) Reaction

See Section III above.

Section 28. (n,np) Reaction.

See Section III above and ref. 46.

Section 51. Inelastic Scattering Exciting First Level in ^{56}Fe

.8611 MeV to 1.5 MeV[7,8]

1.5 MeV to 2.122 MeV[8]

2.122 MeV to 20 MeV[23,31-33,47-51]

Section 52. Inelastic Scattering Exciting First Level in ^{54}Fe

See ref. 35.

Sections 53-76. Inelastic Scattering Exciting Second Through 25th Levels in ^{56}Fe

See refs. 31-33, 47, and 50.

Section 91. Inelastic Scattering Exciting the Continuum

See ENDF/B-IV summary given above and refs. 24, 25, 34, 36, 49, and 52-54.

Section 102. Radiative Capture

See refs. 15-17.

Section 103. (n,p) Reaction

See Section III above and refs. 36 and 37.

Section 104. (n,d) Reaction

See Section III above.

Section 105. (n,t) Reaction

See Section III above.

Section 106. (n,^{3}He) Reaction

See Section III above.

Section 107. (n,α) Reaction

See Section III above and refs. 36 and 38.

File 4. Angular Distribution of Secondary Neutrons

All distributions are given in the center-of-mass system in the Legendre polynomial representation.

Section 2. Elastic Scattering

.00001 eV to 1.23 MeV[7,55-58]

1.23 MeV to 4 MeV[7,55,59-63]

4 MeV to 20 MeV[49,55,64]

Section 16. (n,2n) Reaction

Both neutrons are assumed to be isotropic.

Section 22. (n,nα) Reaction

Assumed isotropic.

Section 28. (n,np) Reaction

Assumed isotropic.

Section 51. Inelastic Scattering Exciting First Level in ^{56}Fe

See refs. 31, 32, and 48-50.

Section 52.   Inelastic Scattering Exciting First Level in ^{54}Fe

Assumed isotropic.

Sections 53-76.   Inelastic Scattering Exciting Second through 25th
Levels in ^{56}Fe

See refs. 31-33 and 48-50.

Section 91.   Inelastic Scattering Exciting the Continuum

Assumed isotropic.

File 5.   Energy Distributions of Secondary Neutrons

Section 16.   (n,2n) Reaction

See summary given above and refs. 45 and 54.

Section 22.   (n,nα) Reaction

See summary given above.

Section 28.   (n,np) Reaction

See summary given above.

Section 91.   Inelastic Scattering Exciting the Continuum

See refs. 24-26, 34, 49, and 51-54.

File 12.   Multiplicities of Gamma Rays Produced by Neutron Reactions

Section 51.   Inelastic Scattering Exciting First Level in ^{56}Fe

Neutron energy is 0.8611 to 2.122 MeV.   One discrete gamma
ray is given.

Section 52.   Inelastic Scattering Exciting First Level in ^{54}Fe

Energy range is 1.433 to 2.122 MeV.   One discrete gamma ray
is given.

Section 102.   Radiative Capture

These gamma rays are given for 19 different neutron energy
ranges.   See Section II above and ref. 65.

File 13.   Gamma-Ray-Production Cross Sections

See summary given above and ref. 22.

File 14.   Angular Distributions of Secondary Gamma Rays

Assumed isotropic.

File 15.   Energy Distributions of Secondary Gamma Rays

See summary given above and references of files 12 and 13.

File 32. Covariances for Resonance Parameters
        See ref. 3.

File 33. Covariances for File 3 Data

REFERENCES

1. S. K. Penny and W. E. Kinney, ORNL-4617 (1971).

2. C. Y. Fu, in *Nuclear Cross Sections for Technology*, Vol. II, p. 651, NBS SP-425, Washington D. C., 1975.

3. C. M. Perey and F. G. Perey, Oak Ridge National Laboratory Report ORNL/TM-6405, ENDF-298 (to be published).

4. F. M. Mann, Hanford Engineering Development Laboratory, private communication (1976).

5. R. E. Maerker *et al.*, Oak Ridge National Laboratory Report ORNL-5013 (1976).

6. A. B. Smith and J. F. Whalen, Argonne National Laboratory, ANL/NDM-34 (1977).

7. W. E. Kinney and F. G. Perey, Nucl. Sci. Eng. 63, 418 (1977).

8. F. Voss *et al.*, USAEC CONF-710310, p. 218 (1971).

9. A. B. Smith, Argonne National Laboratory, private communication (1976).

10. D. L. Smith, Argonne National Laboratory Report ANL/NDM-20 (1976).

11. S. N. Cramer and E. M. Oblow, Oak Ridge National Laboratory Report ORNL/TM-5548 (1976).

12. G. L. Morgan and F. G. Perey, Oak Ridge National Laboratory Report ORNL/TM-4193 (1975).

13. J. Frehaut and G. Mosinski, p. 855, Conference on Nuclear Cross Sections and Technology, NBS Special Publication 425 (1975).

14. R. H. Johnson, University of Illinois, private communication (1975).

15. B. J. Allen *et al.*, Nucl. Phys. A269, 408 (1976). Also "Valence Neutron Capture in ^{56}Fe," to be published.

16. C. Le Rigoleur *et al.*, Centre d'Etudes Nucléaires de Cadarache, CEA-R-4788 (1976).

17. D. I. Garber and R. R. Kinsey, Brookhaven National Laboratory Report BNL-325, third edition, volume II (1976).

18. W. E. Kinney and F. G. Perey, Oak Ridge National Laboratory, private communication (1977).

19. P. G. Young, Los Alamos National Laboratory, private communication (1976).

20. V. J. Orphan *et al.*, Gulf Radiation Technology GRT-A10743 (1971), revised by V. C. Rogers, Intelcom Radiation Technology, private communication (1973).

21. J. K. Dickens *et al.*, Oak Ridge National Laboratory Report ORNL-4798 (1973).

22. G. T. Chapman and G. L. Morgan, Oak Ridge National Laboratory ORNL/TM-5416 (1976).

23. A. B. Smith, Argonne National Laboratory, private communication (1973).

24. J. L. Kammerdiener, UCRL-51232 (1972).

25. G. Clayeux *et al.*, CEA-R-4279 (1972).

26. L. F. Hansen *et al.*, Nucl. Sci. Eng. 51, 278 (1973).

27. S. N. Cramer *et al.*, ORNL-TM-4072 (1973).

28. V. J. Orphan *et al.*, GRT-A10743 (1971), rev. by V. Rogers, IRT, private communication (1973).

29. J. K. Dickens *et al.*, Nucl. Sci. Eng. 50, 311 (1973).

30. J. A. Harvey, USAEC Conf-720901, p. 1075 (1972).

31. S. K. Penny, Computer Code HELGA, ORNL (1973).

32. R. H. Bassel *et al.*, Computer Code JULIE, ORNL (1966).

33. G. S. Mani, Nucl. Phys. A165, 225 (1971).

34. C. Y. Fu, Computer Code NNNGAM, ORNL (1973).

35. W. E. Kinney and F. G. Perey, ORNL-4907 (1973).

36. M. D. Goldberg *et al.*, BNL-325 (1966).

37. J. C. Robertson *et al.*, J. Nucl. Energy 27, 139 (1973).

38. G. J. Kirouac and C. J. Slavik, private communication (1972).

39. S. Pearlstein, BNL-16271 (1971).

40. J. J. Schmidt, KFK-120 (1966).

41. J. S. Story, UDAEA Winfrith, private communication (1970).

42. A. D. Carlson and R. J. Cerbone, GA-9149 (1969).

43. S. Cierjacks *et al.*, KFK-1000 (1968).

44. D. C. Irving and E. A. Straker, ORNL-TM-2891 (1970).

45. O. A. Salnikov *et al.*, Soviet J. of Nucl. Phys. 12, 620 (1971).

46. D. L. Allan, Nucl. Phys. 24, 274 (1961).

47. W. B. Gilboy and J. B. Towle, Nucl. Phys. 64, 130 (1965).

48. A. Gilbert and A. G. W. Cameron, Can. J. Phys. 43, 1446 (1965).

49. W. E. Kinney and F. G. Perey, ORNL-4515 (1970).

50. M. N. Rao, Nucl. Data Sheets B3-3, 4-43 (1970).

51. R. J. Peterson, Annals of Physics 53, 40 (1969).

52. G. C. Bonazzola *et al.*, Nucl. Phys. 51, 353 (1963).

53. R. M. Schectman and J. D. Anderson, Phys. Rev. 77, 241 (1965).

54. S. C. Mathur *et al.*, Phys. Rev. 186, 1038 (1969).

55. E. Barnard *et al.*, PEL-180, Pelindaba, Pretoria (1968).

56. S. A. Cox, Bull. Am. Phys. Soc. 8, 478 (1963).

57. I. O. Korzh and M. T. Skylar, UKR. Fiz. Ah. 8, 1389 (1963).

58. M. V. Pasechnik *et al.*, At. En. USSR 16, 207 (1964).

59. J. R. Beyster *et al.*, Phys. Rev. 104, 1319 (1956).

60. R. L. Becker *et al.*, Nucl. Phys. 89, 154 (1966).

61. N. A. Bostron *et al.*, WADC-TR-59-31 (1959).

62. L. Cranberg and J. S. Levin, Phys. Rev. 103, 343 (1969).

63. B. Holmqvist, Arkiv Fysik 38, 403 (1968).

64. F. G. Perey, Computer Code GENOA, ORNL (1970).

65. J. E. White *et al.*, Nucl. Sci. Eng. 51, 496 (1973).
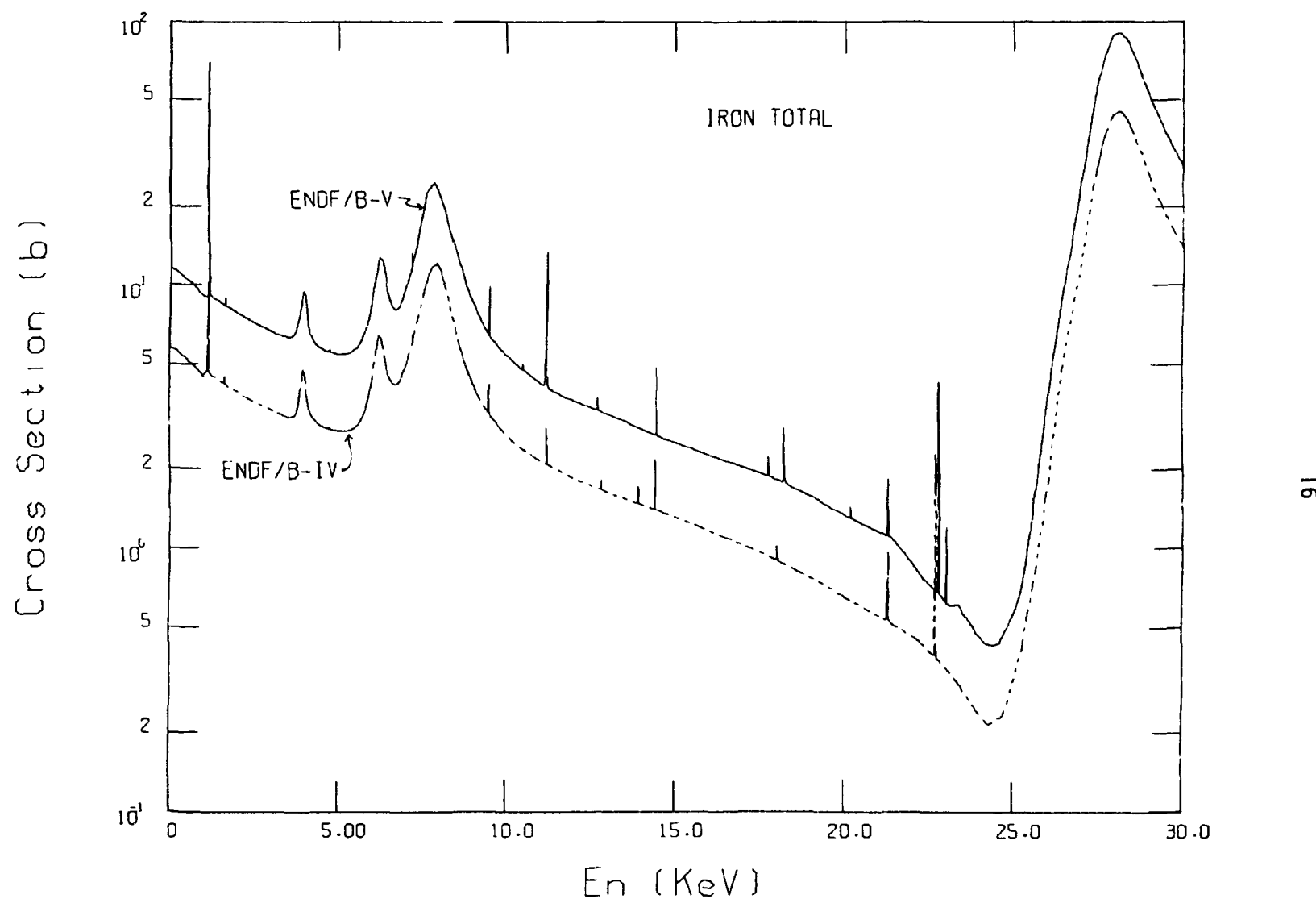
Fig. 1. Comparison of ENDF/3-V Fe total cross sections with ENDF/B-IV.
The ENDF/B-IV values are divided by 2.
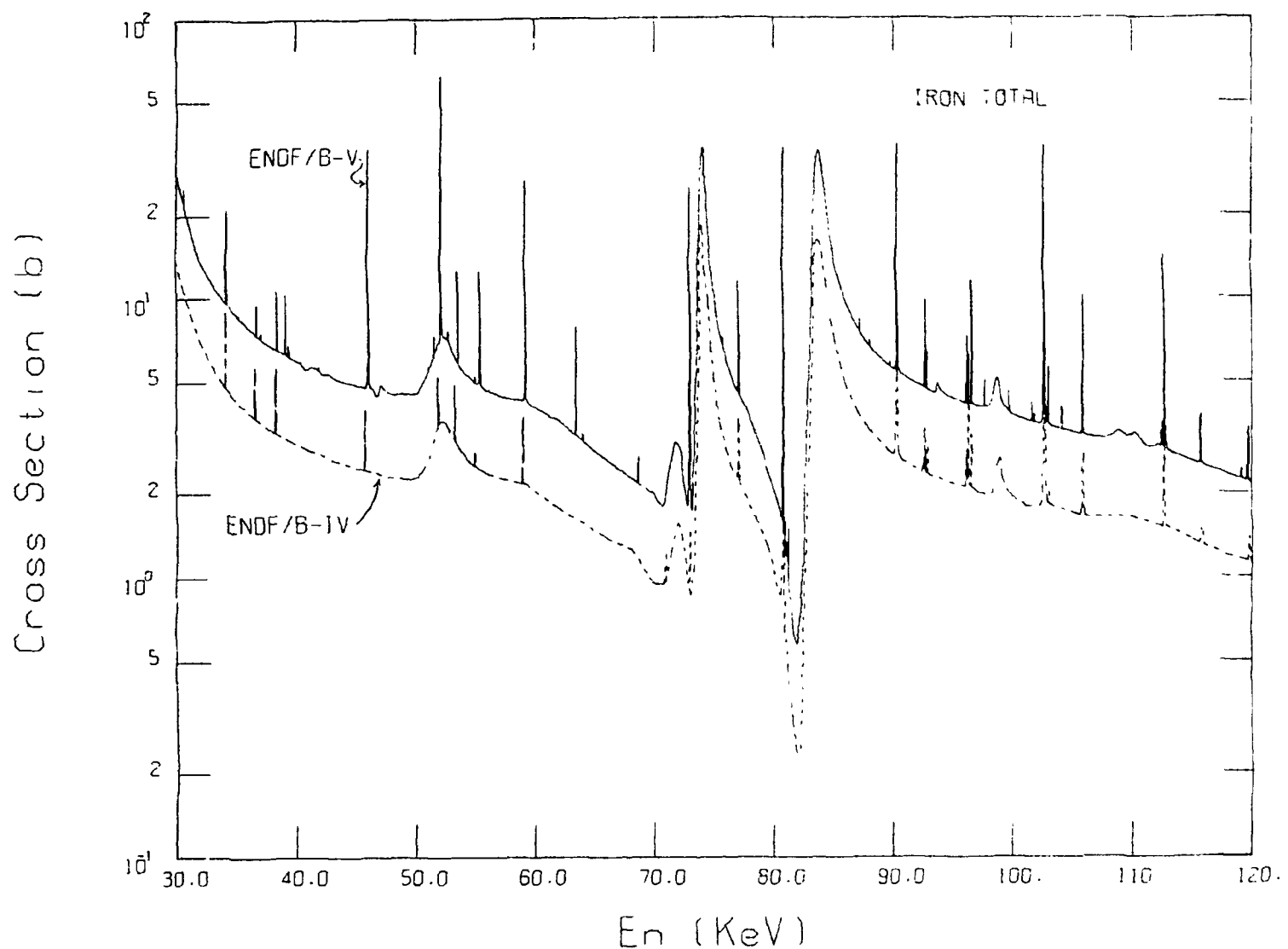
Fig. 2. Comparison of ENDF/B-V Fe total cross sections with ENDF/B-IV.
The ENDF/B-IV values are divided by 2.
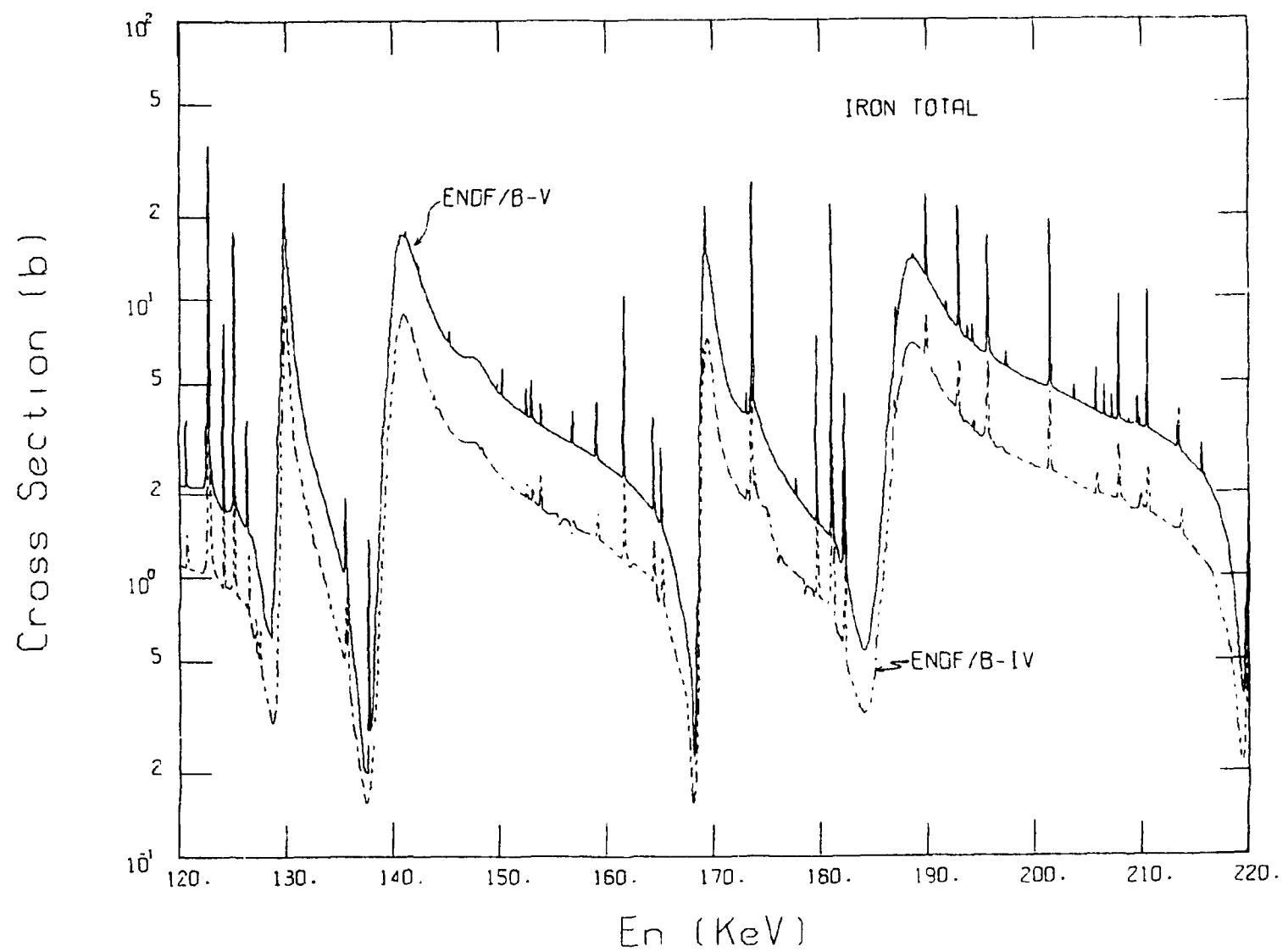
Fig. 3. Comparison of ENDF/B-V Fe total cross sections with ENDF/B-IV.
The ENDF/B-IV values are divided by 2.
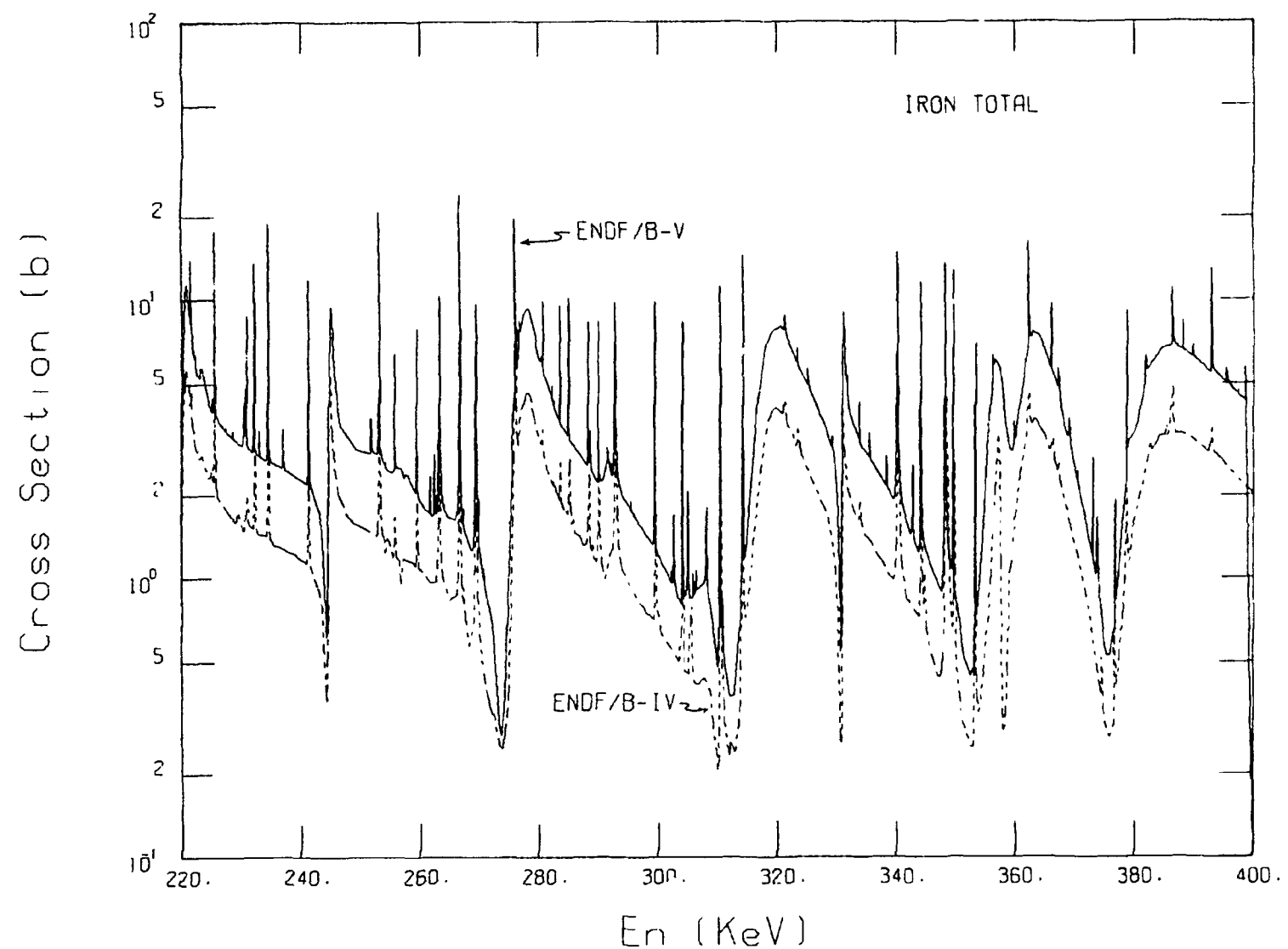
Fig. 4. Comparison of ENDF/B-V Fe total cross sections with ENDF/B-IV.
The ENDF/B-IV values are divided by 2.
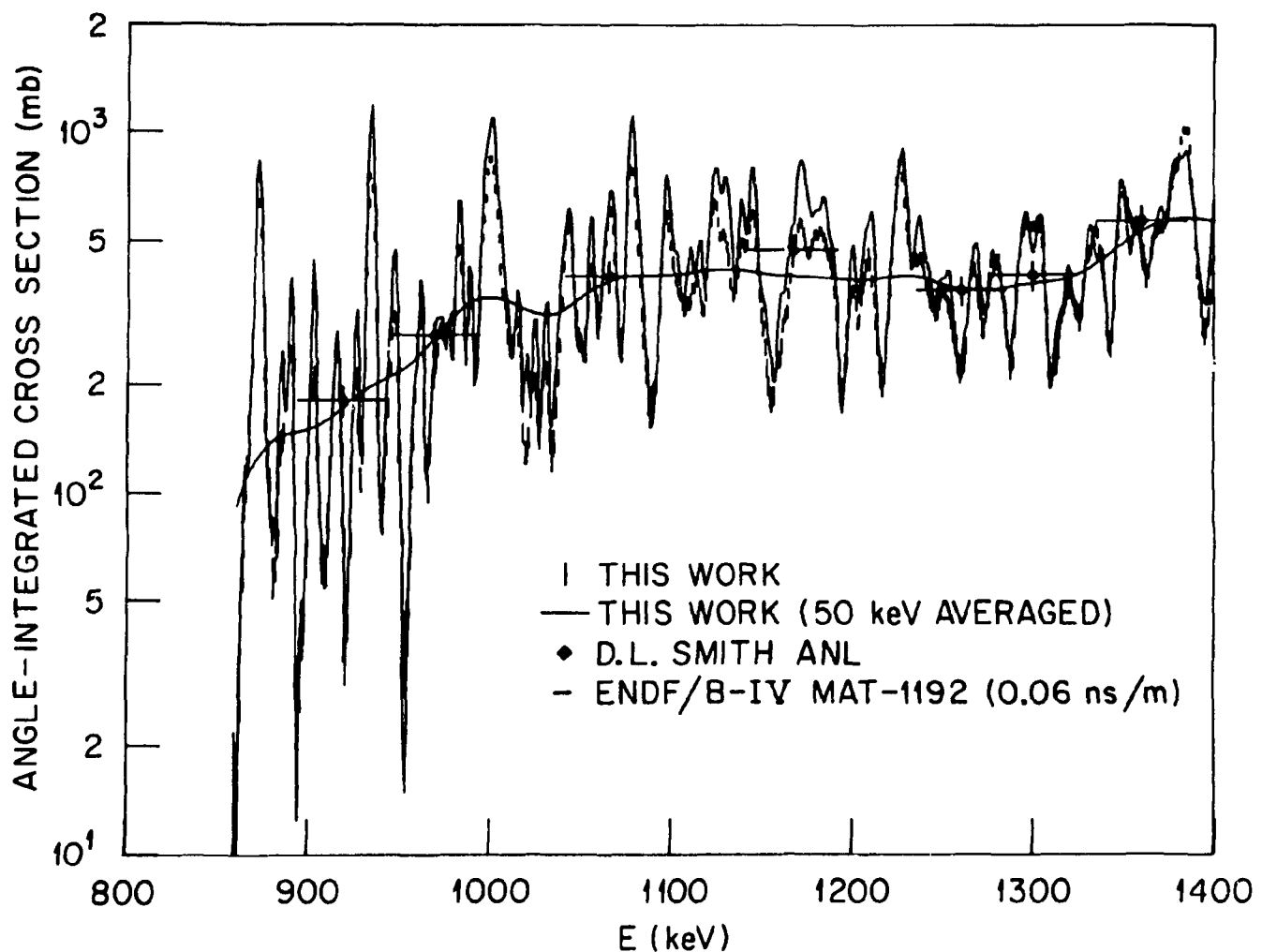
Fe 846 keV Level Cross Section.

Fig. 5. Inelastic scattering cross sections exciting the 846-keV level for ENDF/B-V were taken from the work of Kinney and Perey[7] (broken lines), from which this figure was reproduced. Fine-structured solid line is ENDF/B-IV, MAT 1192.
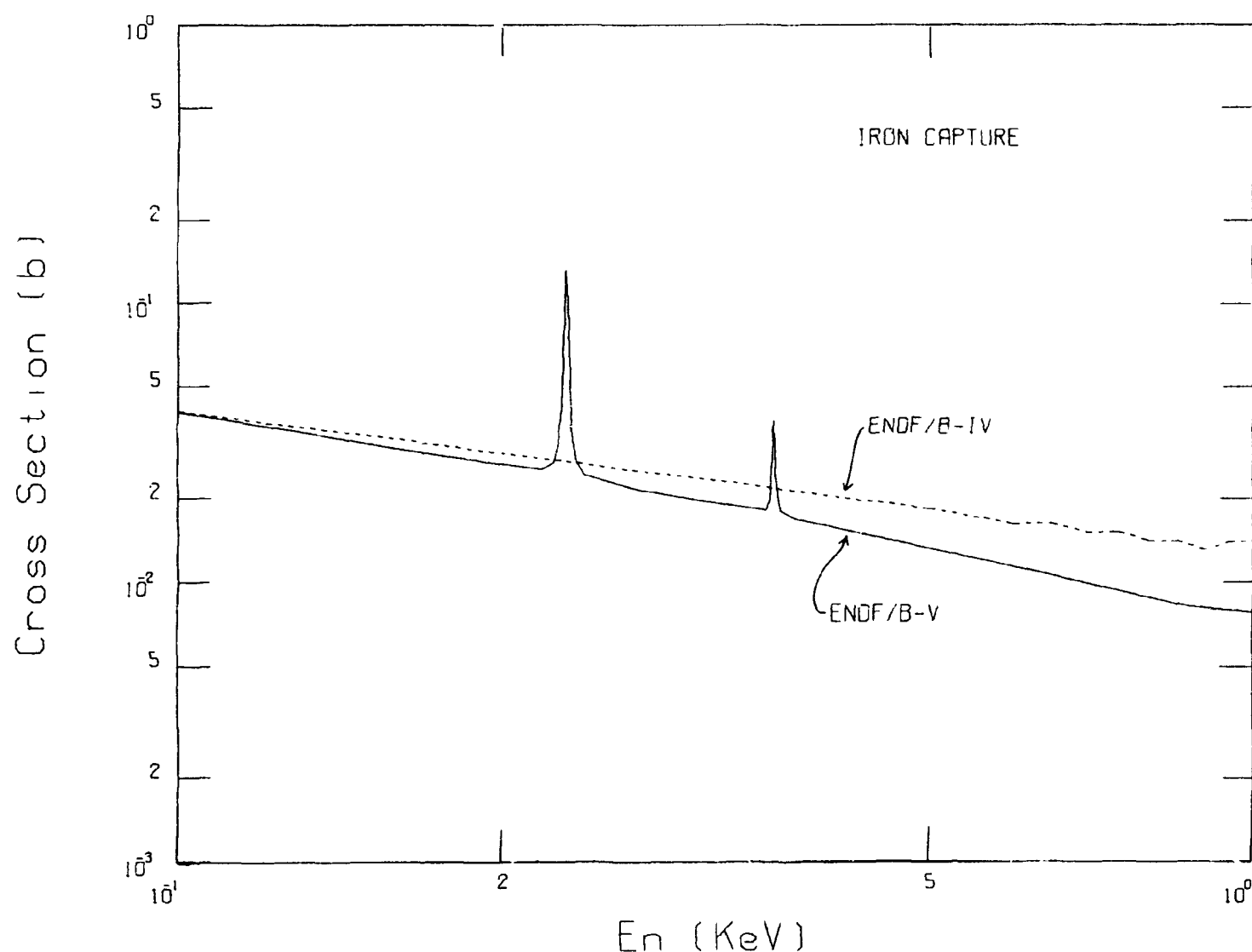
Fig. 6. Comparison of ENDF/B-V Fe Capture cross sections with ENDF/B-IV.
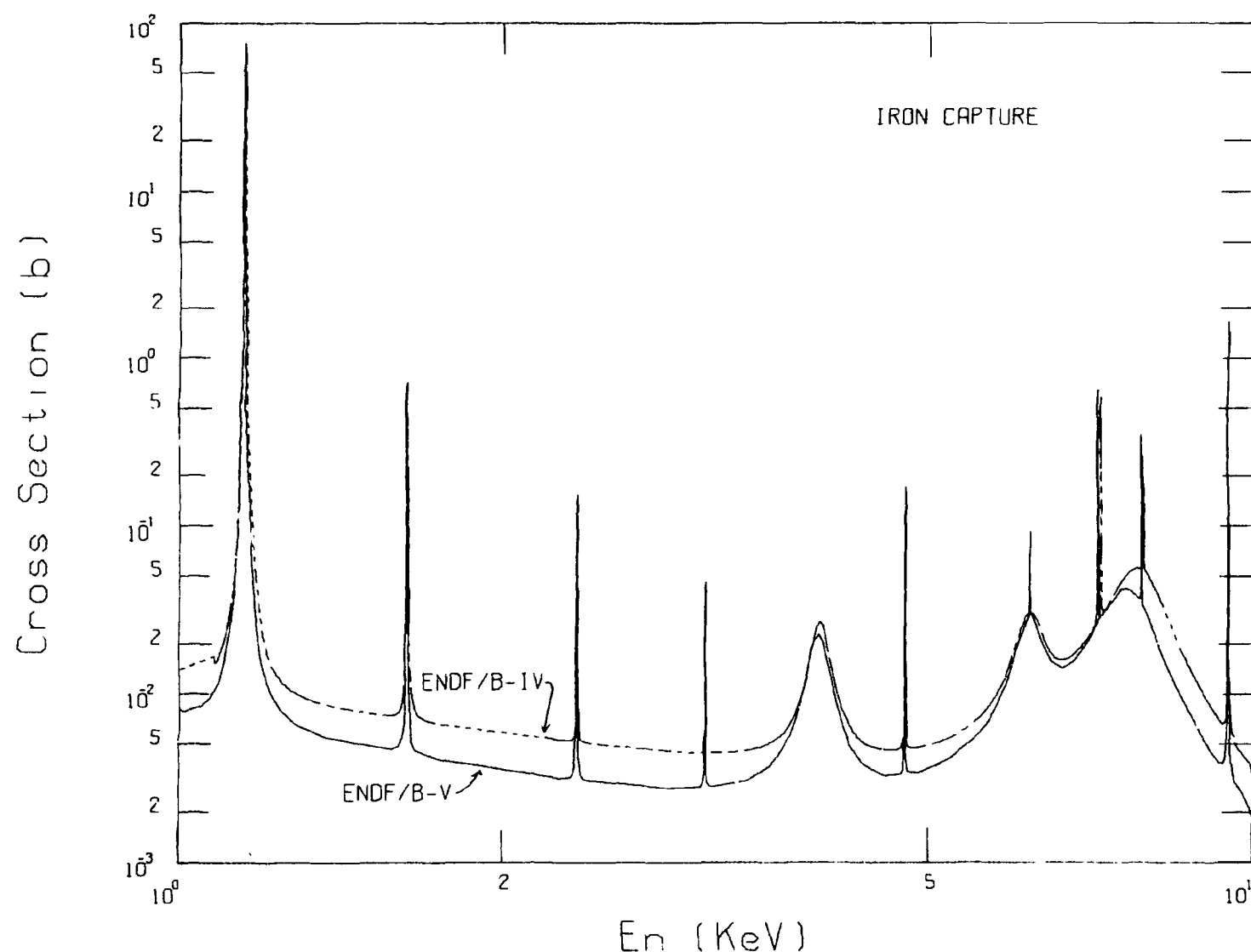
Fig. 7. Comparison of ENDF/B-V Fe Capture cross sections with ENDF/B-IV.
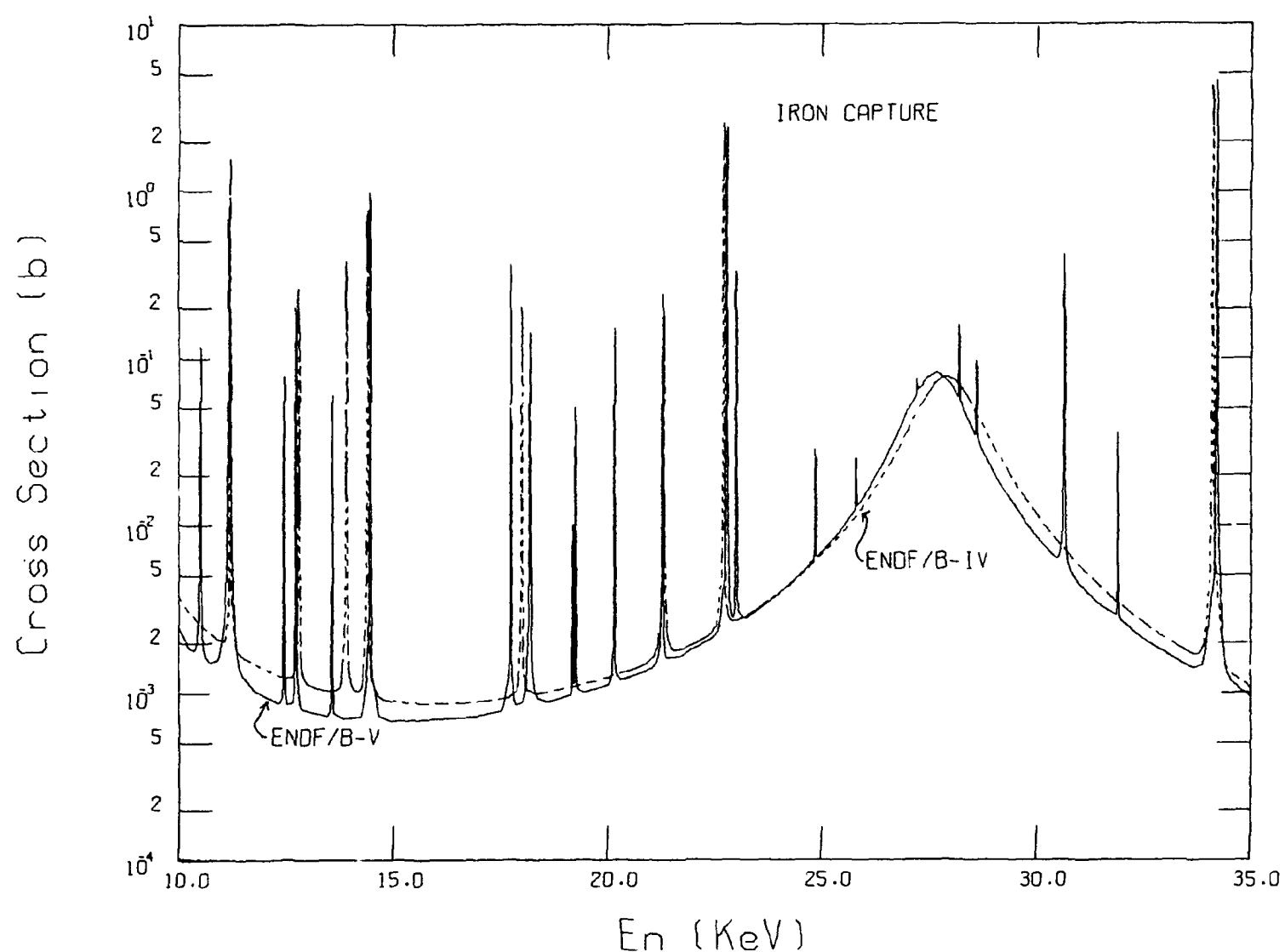
Fig. 8. Comparison of ENDF/B-V Fe Capture cross sections with ENDF/B-IV.
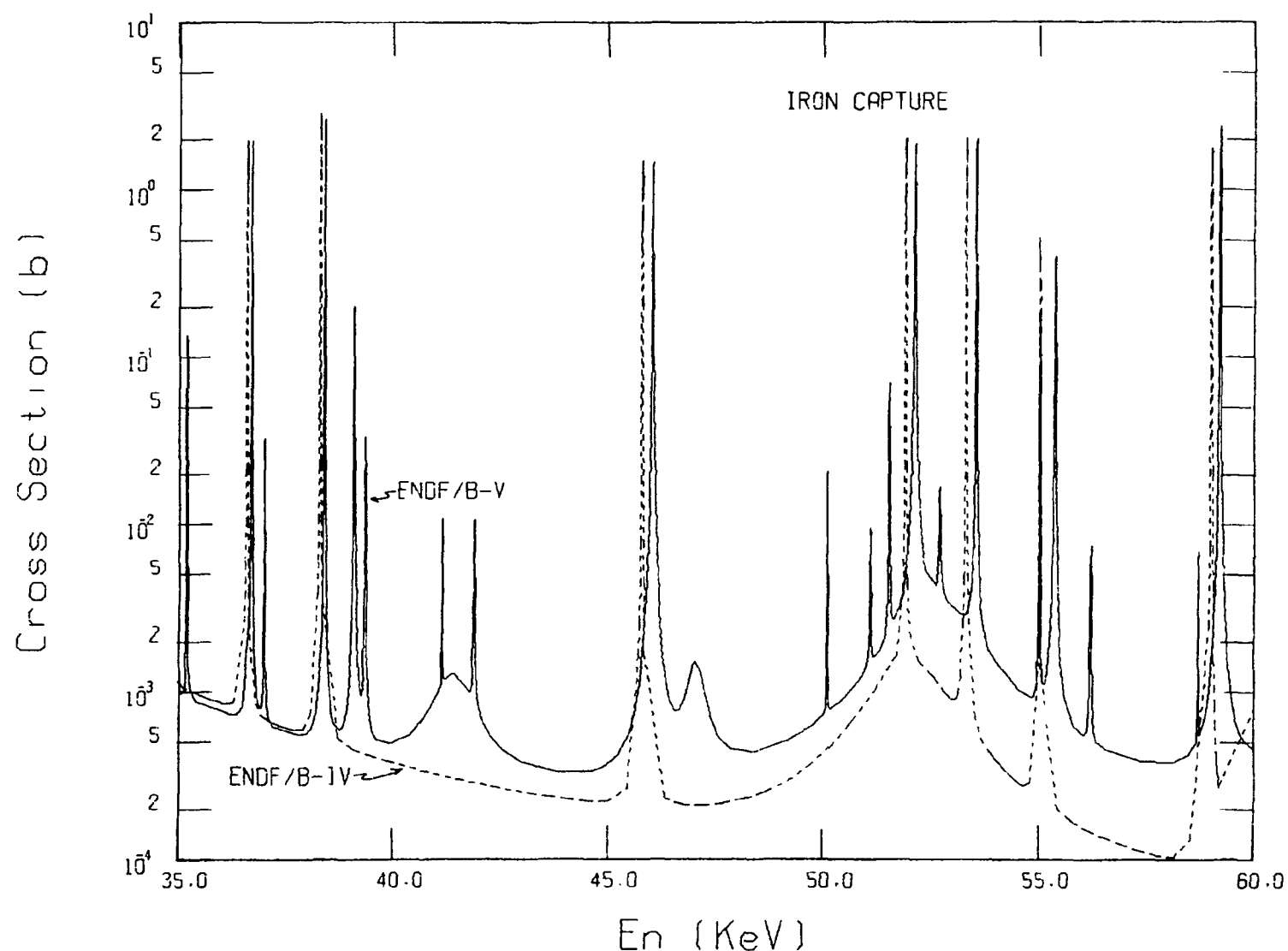
Fig. 9. Comparison of ENDF/B-V Fe Capture cross sections with ENDF/B-IV.
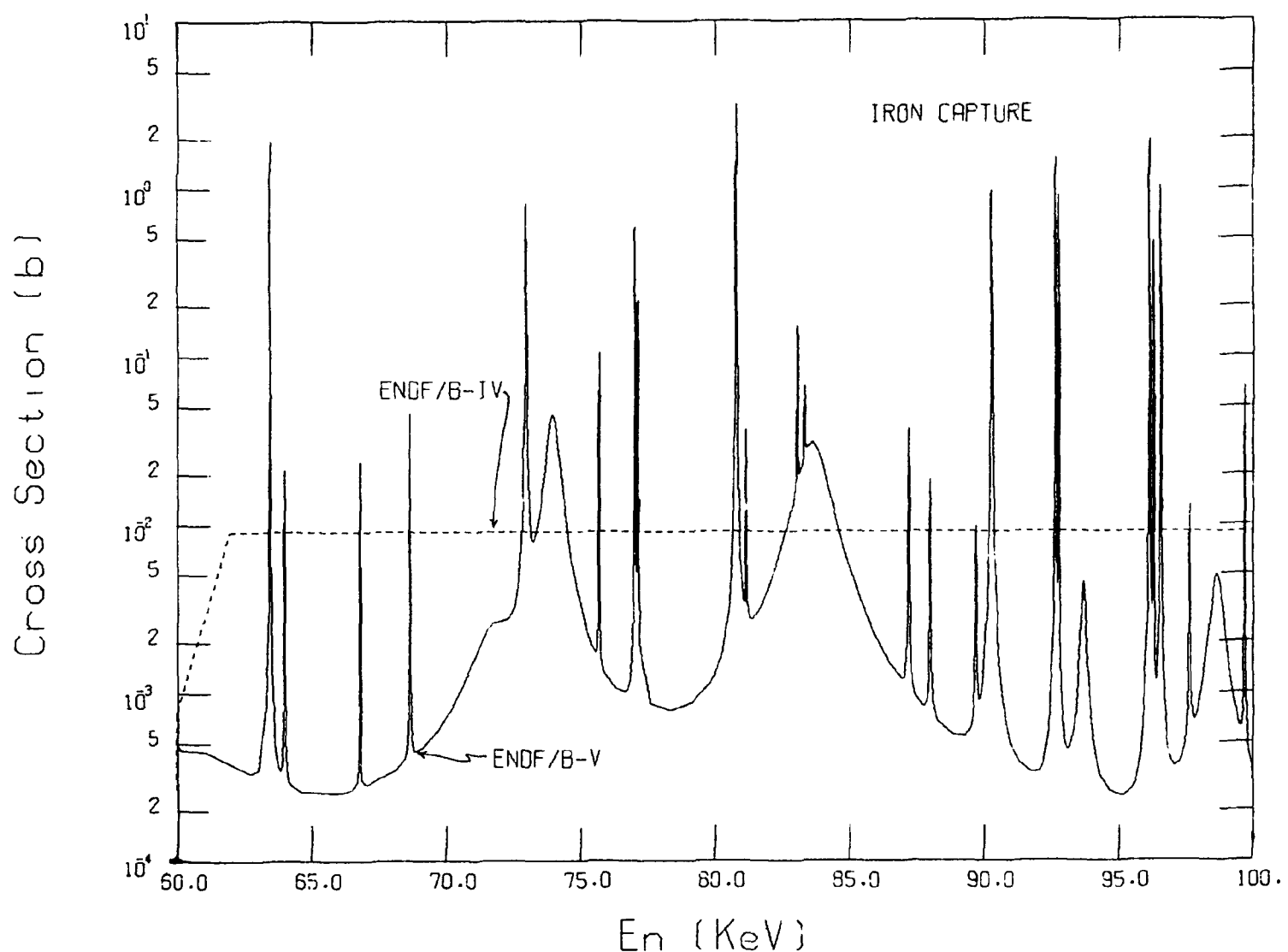
Fig. 10. Comparison of ENDF/B-V Fe Capture cross sections with ENDF/B-IV.
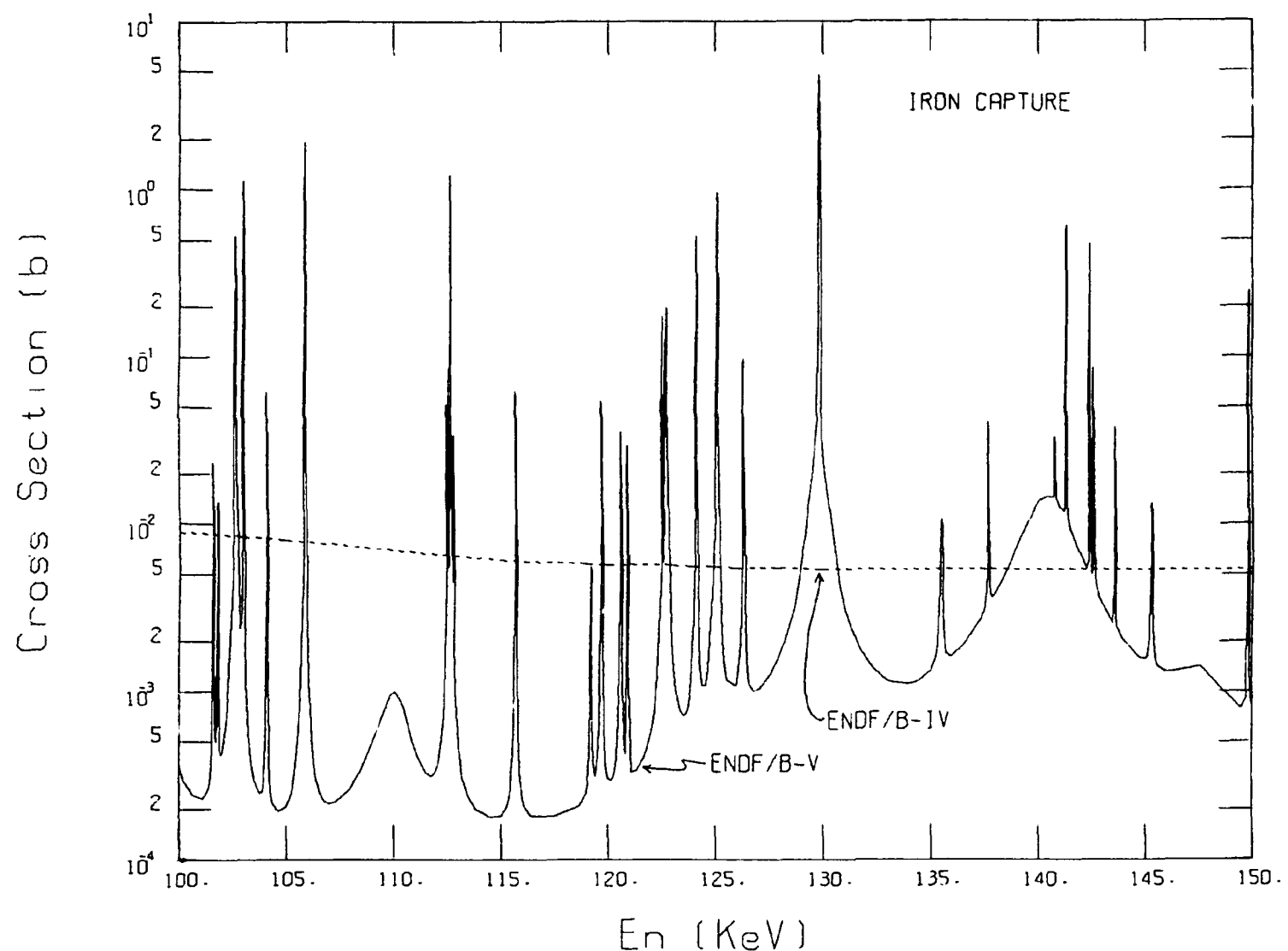
Fig. 11. Comparison of ENDF/B-V Fe Capture cross sections with ENDF/B-IV.
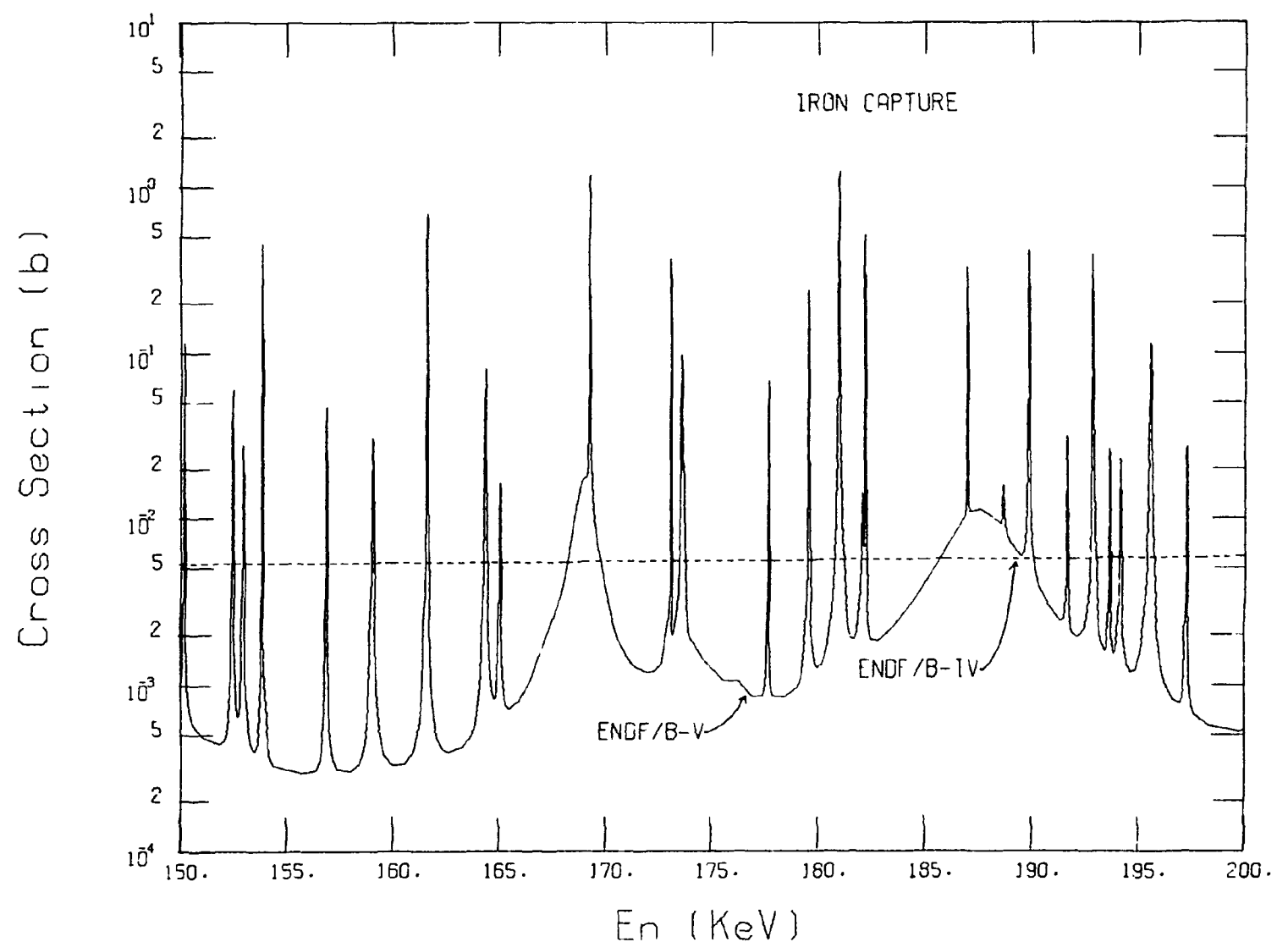
Fig. 12. Comparison of ENDF/B-V Fe Capture cross sections with ENDF/B-IV.
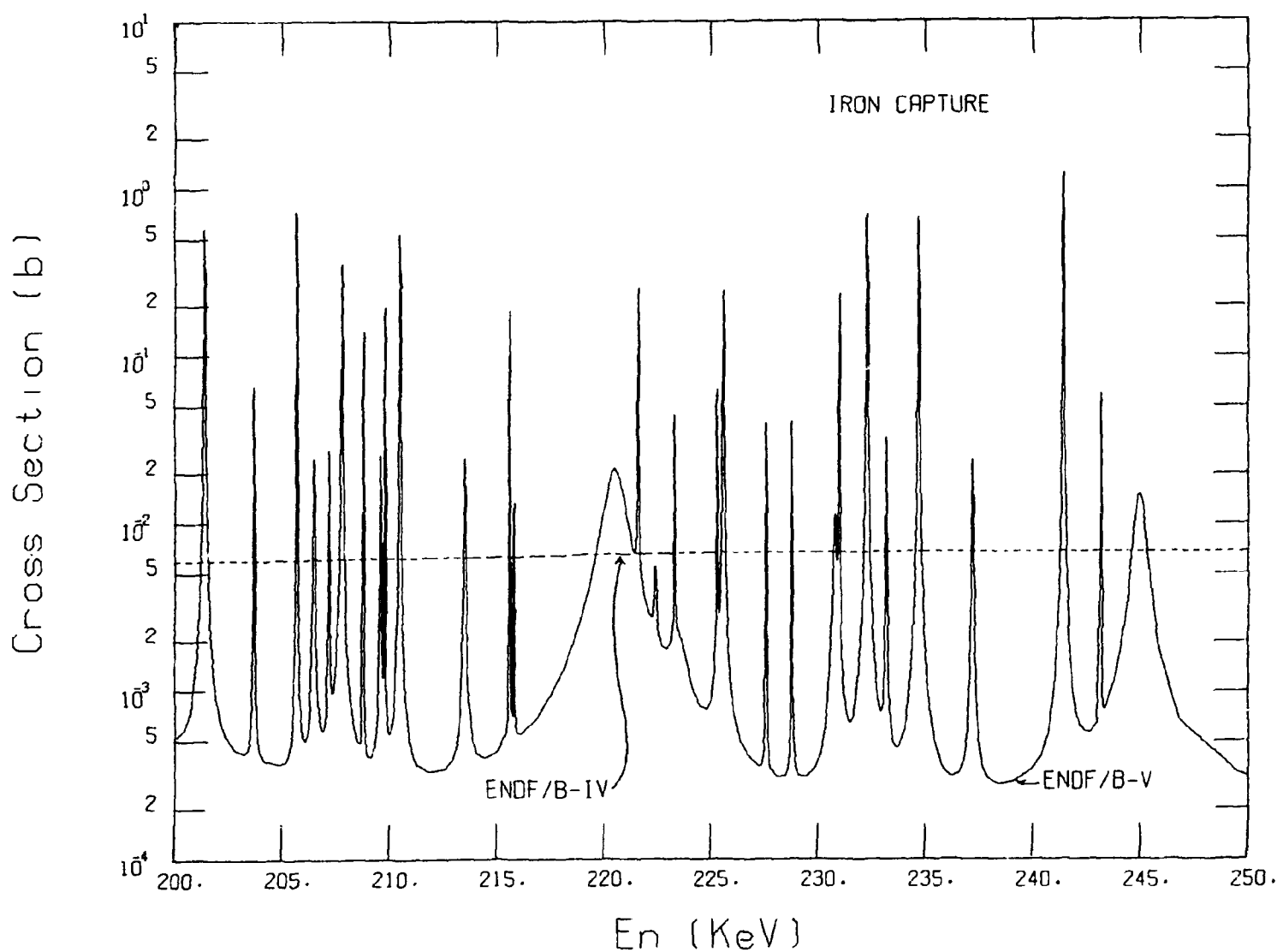
Fig. 13. Comparison of ENDF/B-V Fe Capture cross sections with ENDF/B-IV.
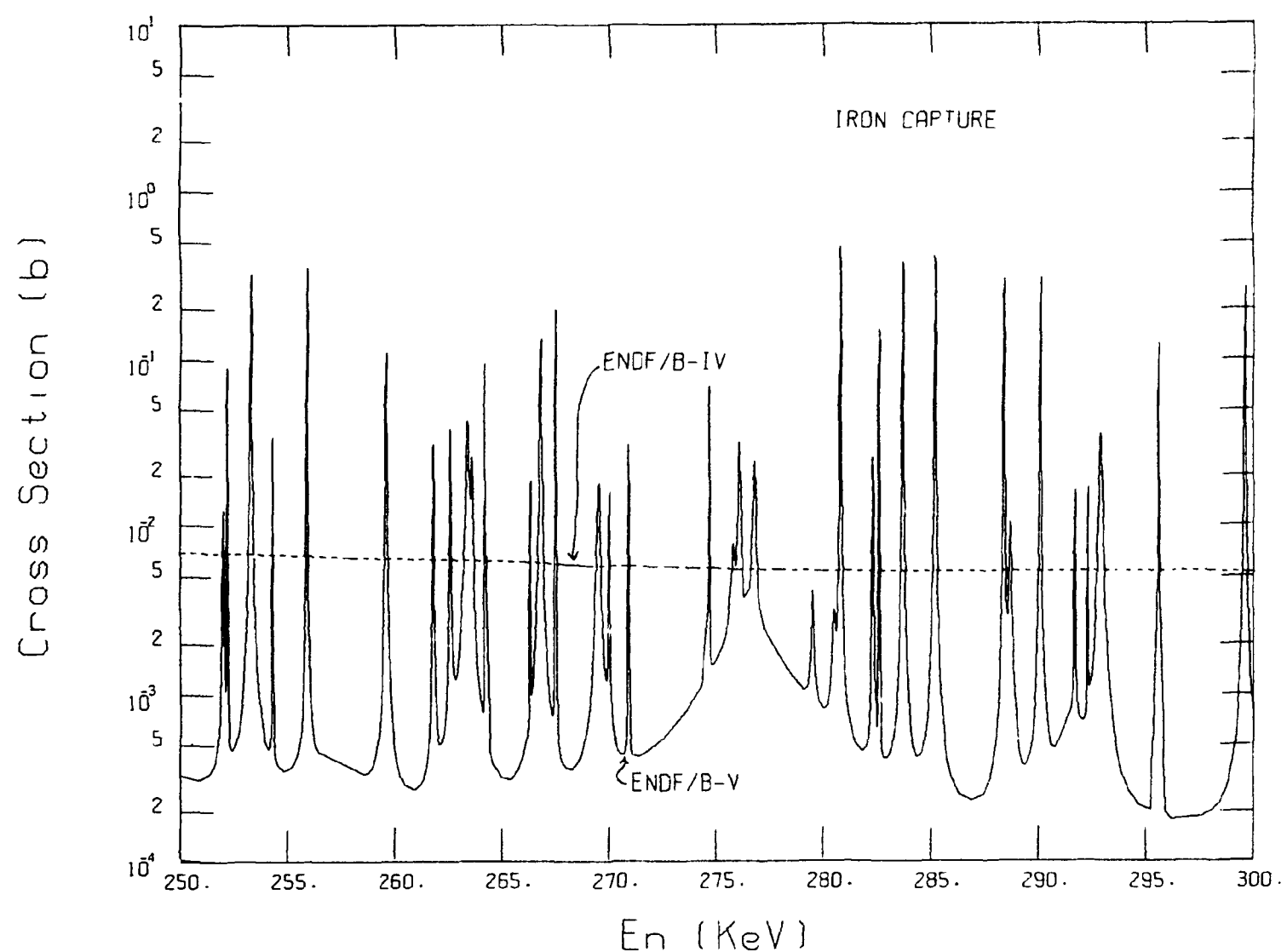
Fig. 14. Comparison of ENDF/B-V Fe Capture cross sections with ENDF/B-IV.
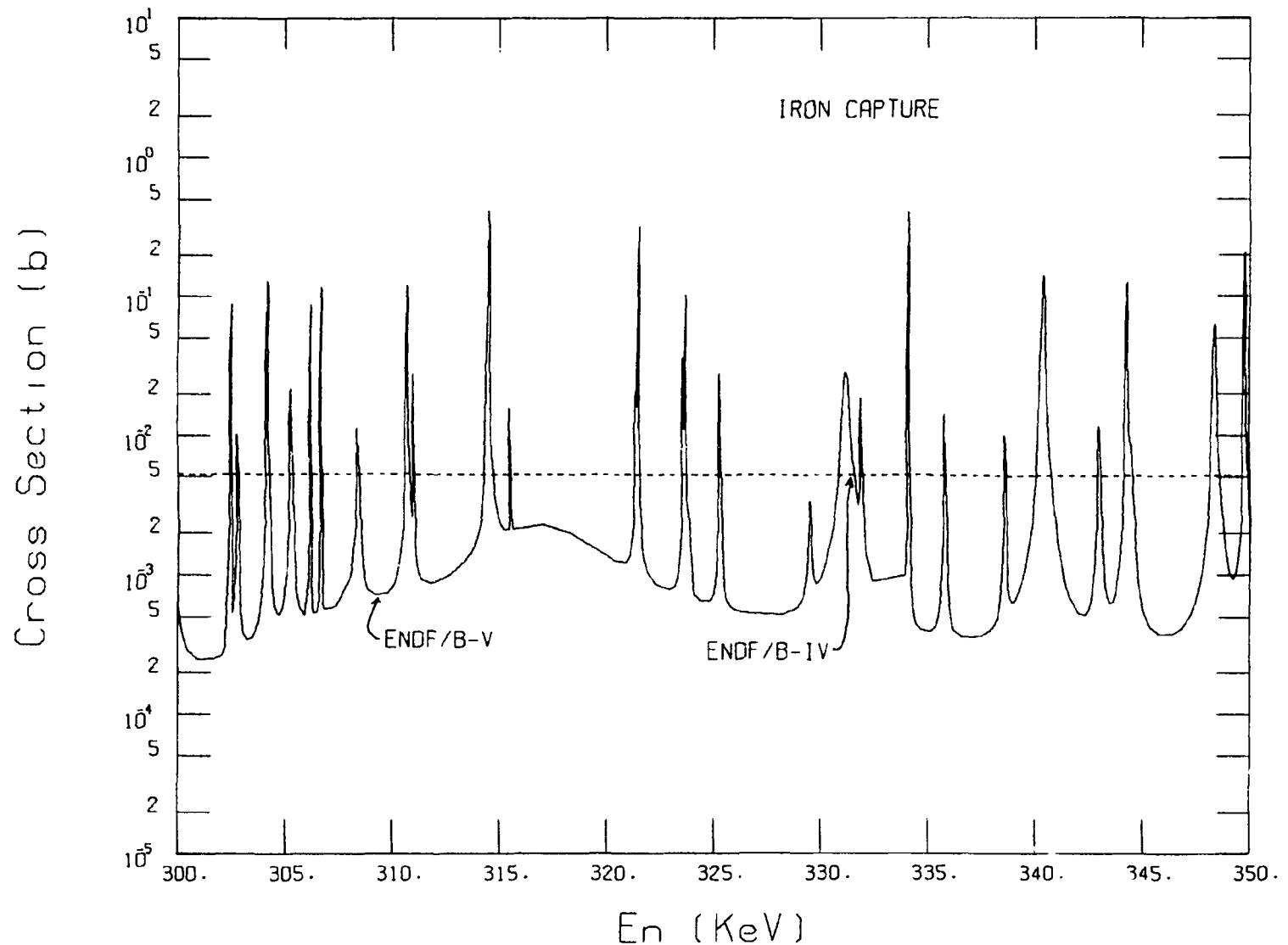
Fig. 15. Comparison of ENDF/B-V Fe Capture cross sections with ENDF/B-IV.
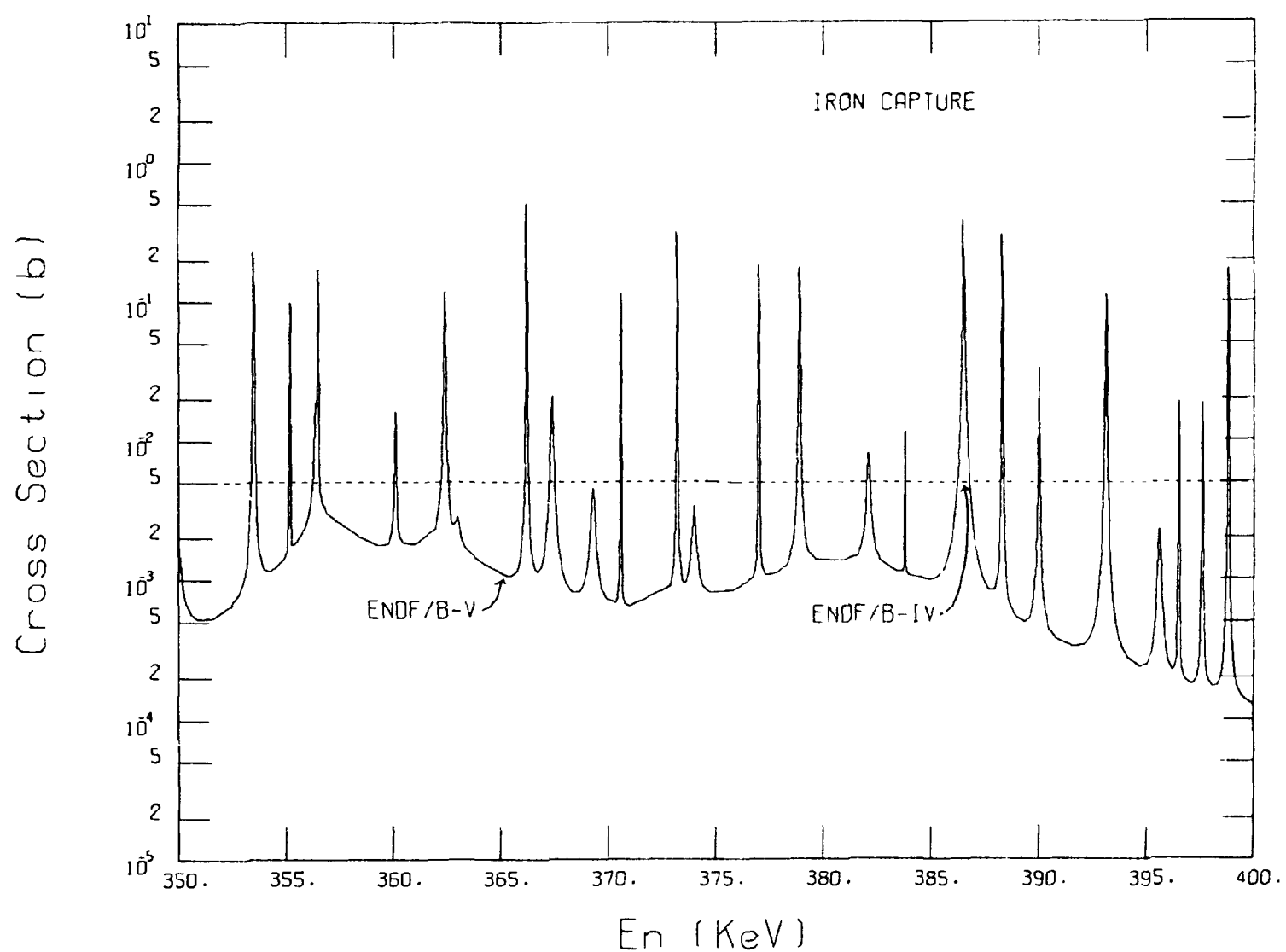
Fig. 16. Comparison of ENDF/B-V Fe Capture cross sections with ENDF/B-IV.
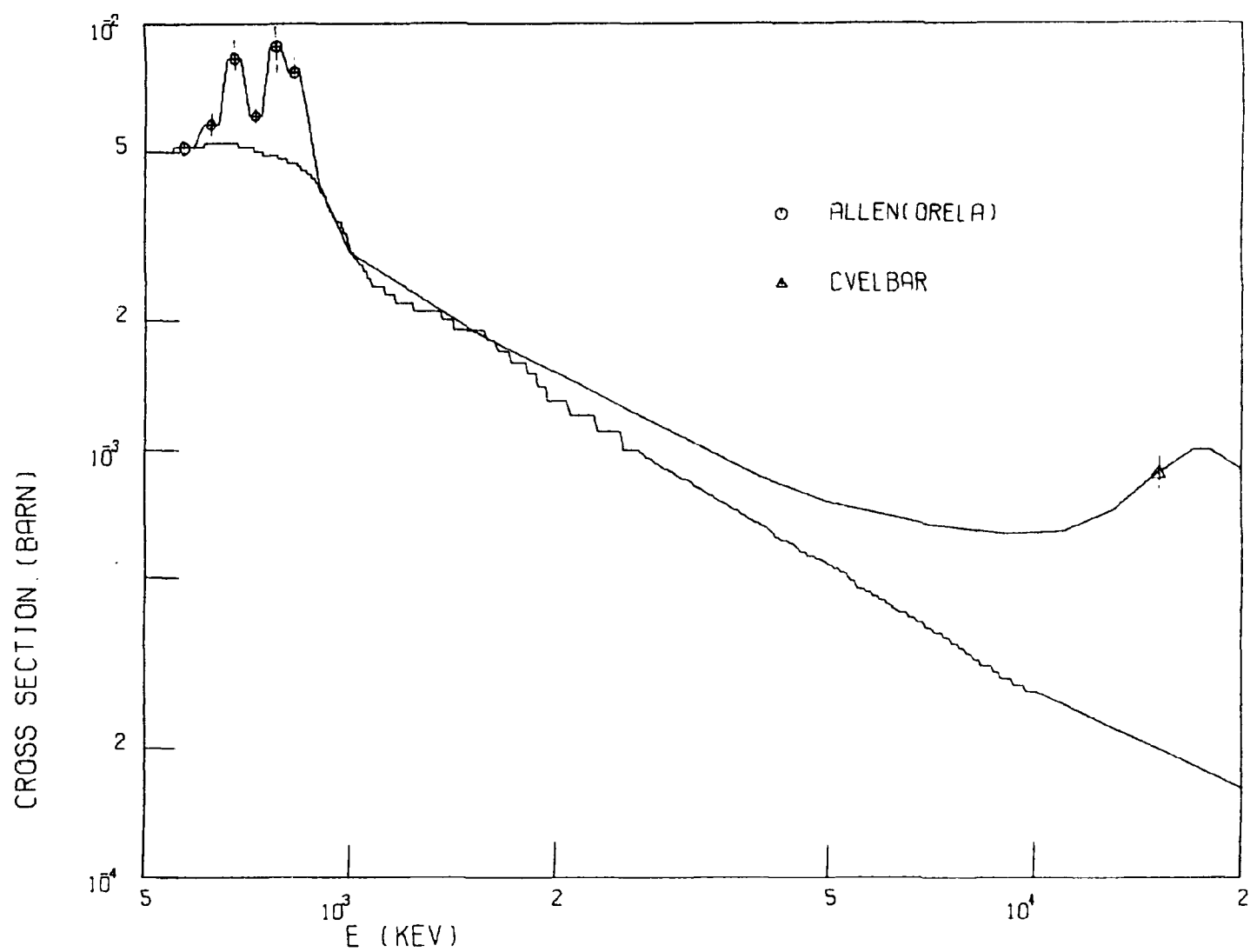
Fig. 17. Comparison of ENDF/B-V Fe capture cross sections with ENDF/B-IV (lower curve).
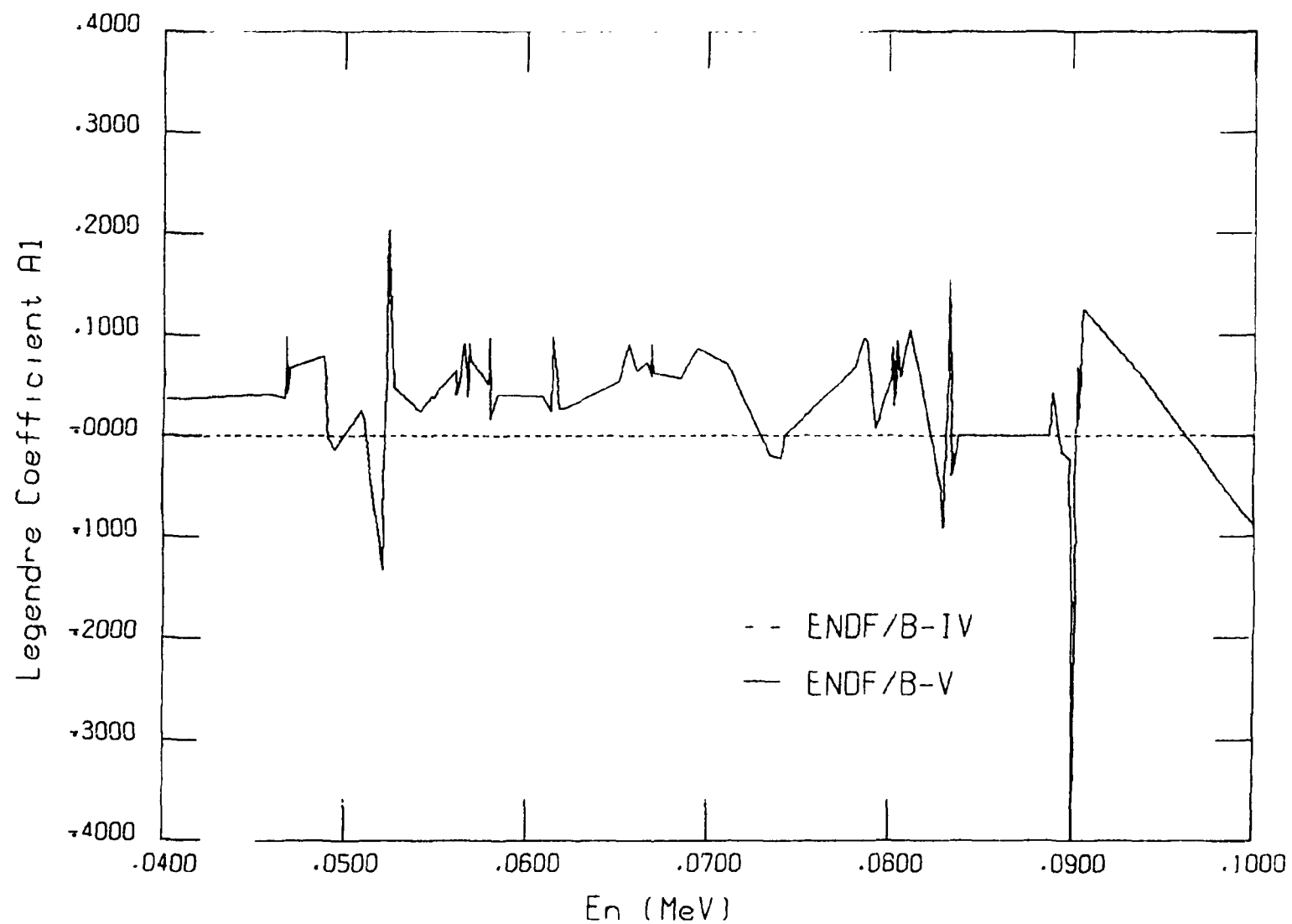
Fig. 18. Comparison of ENDF/B-V Al Legendre coefficients for the angular distributions of elastically scattered neutrons with ENDF/B-IV from 40 keV to 100 keV.
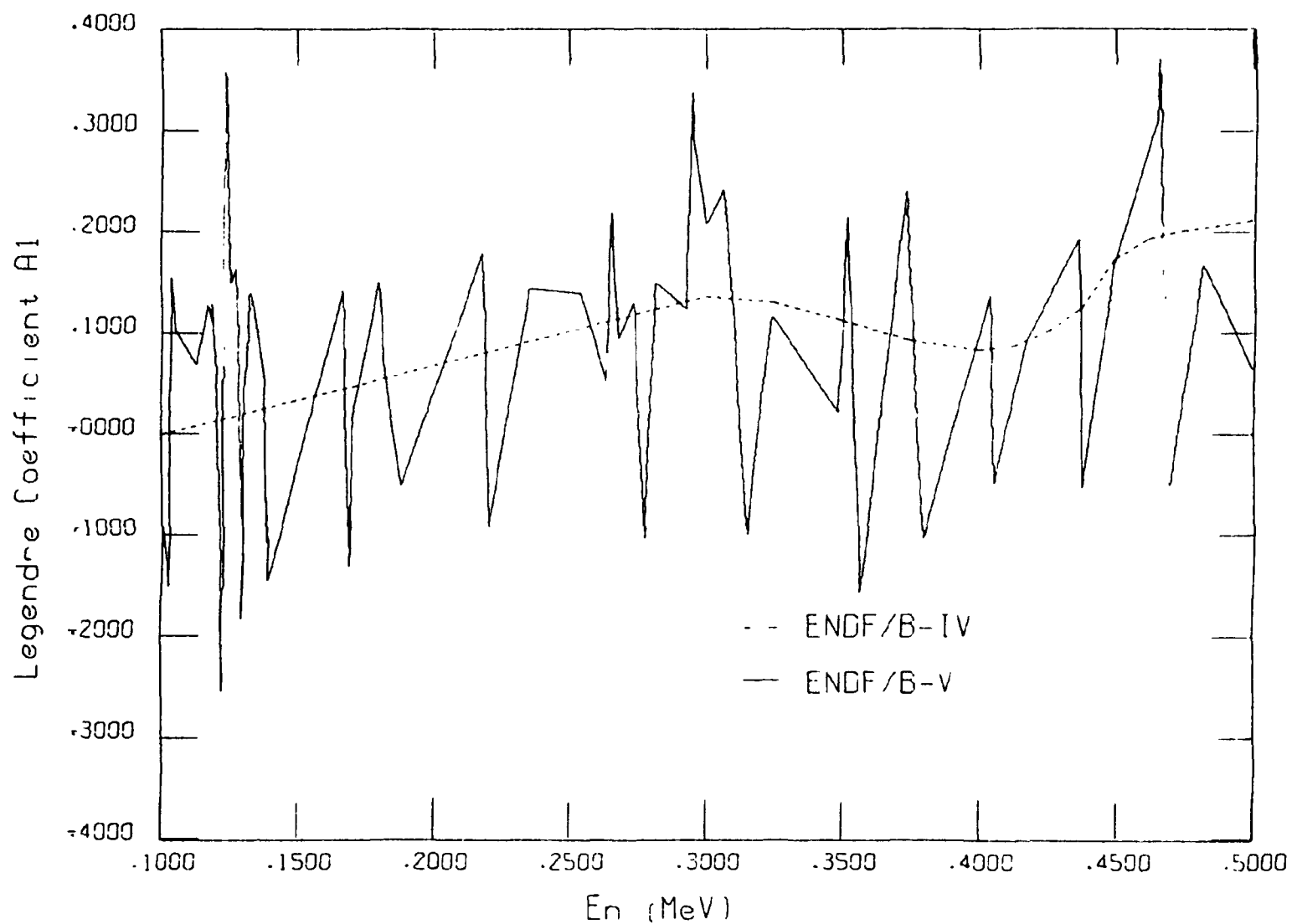
Fig. 19. Comparison of ENDF/B-V Al Legendre coefficients for the angular distributions of elastically scattered neutrons with ENDF/B-IV from 100 keV to 500 keV.
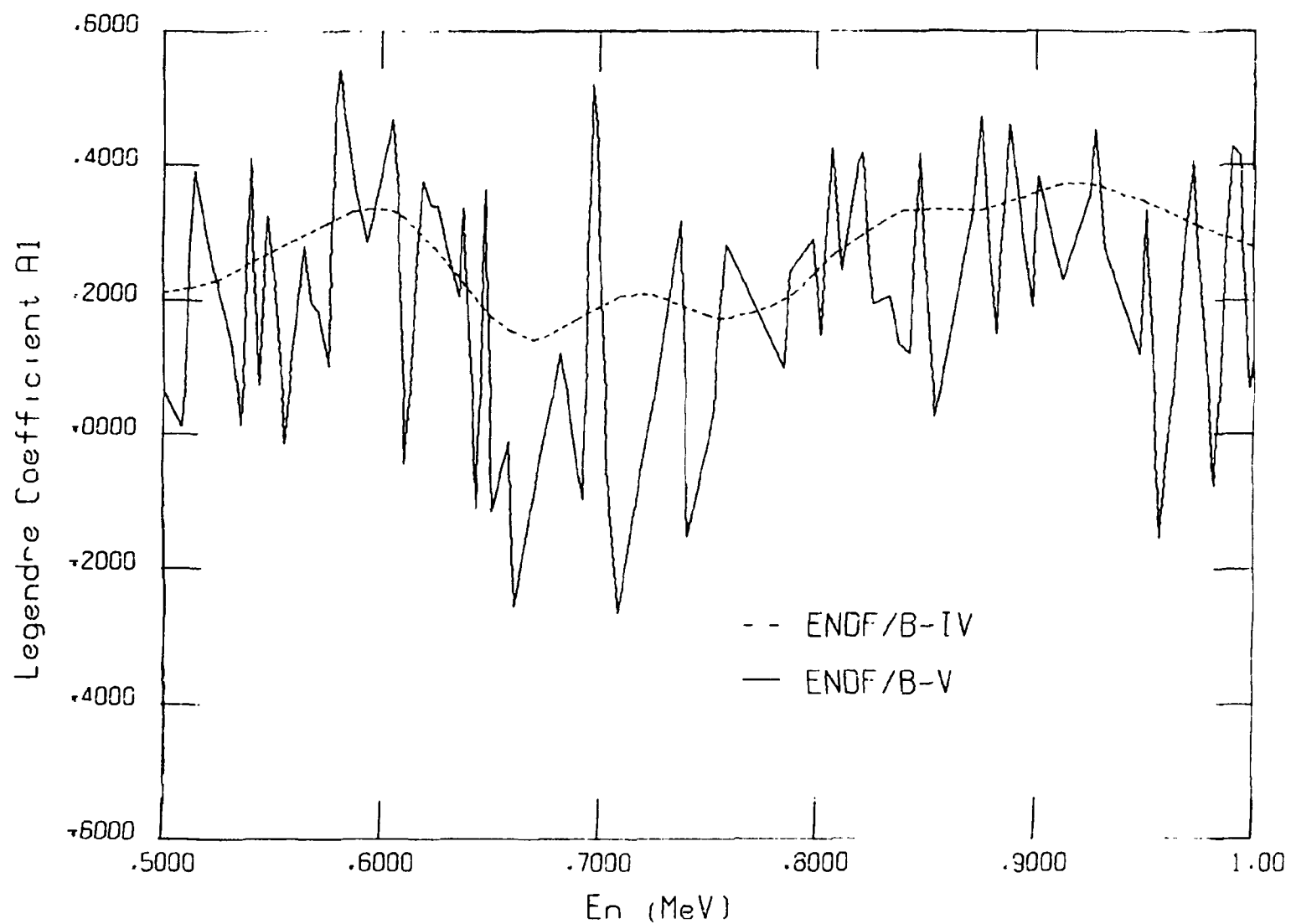
Fig. 20. Comparison of ENDF/B-V Al Legendre coefficients for the angular distributions of elastically scattered neutrons with ENDF/B-IV from 500 keV to 1 MeV.
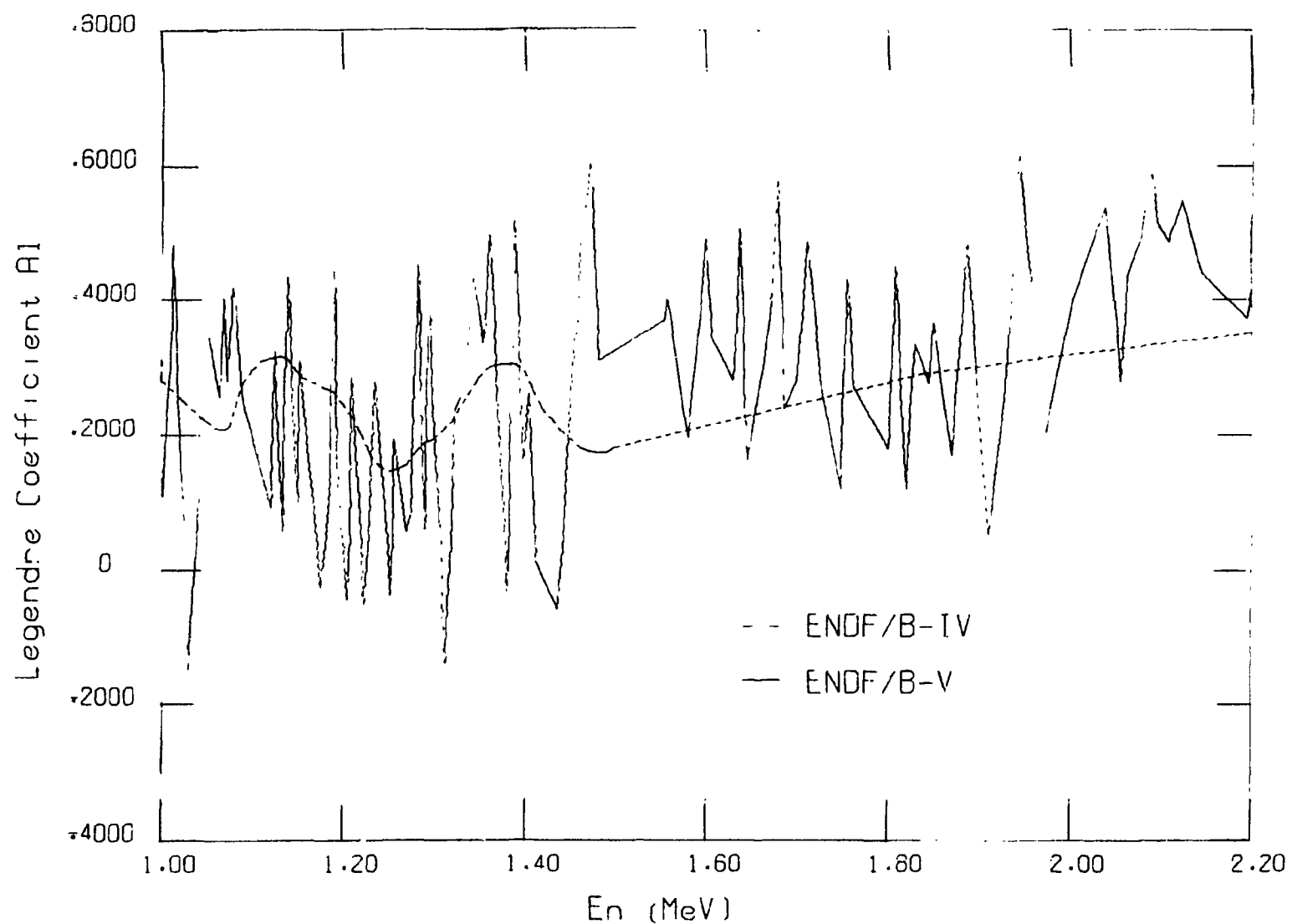
Fig. 21. Comparison of ENDF/B-V Al Legendre coefficients for the angular distributions of elastically scattered neutrons with ENDF/B-IV from 1 MeV to 2.2 MeV.
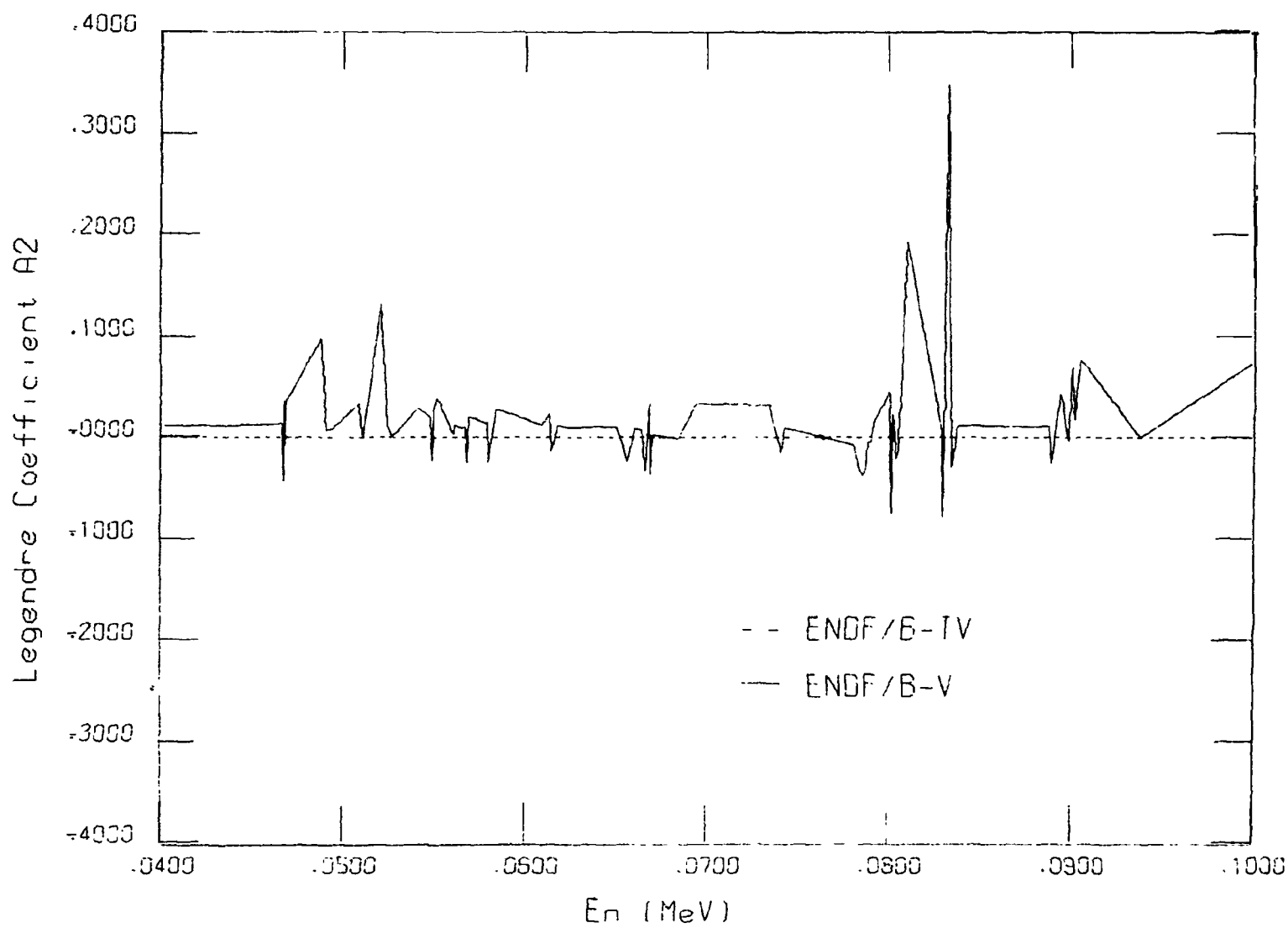
Fig. 22. Comparison of ENDF/B-V A2 Legendre coefficients for the angular distributions of elastically scattered neutrons with ENDF/B-IV from 40 keV to 100 keV.
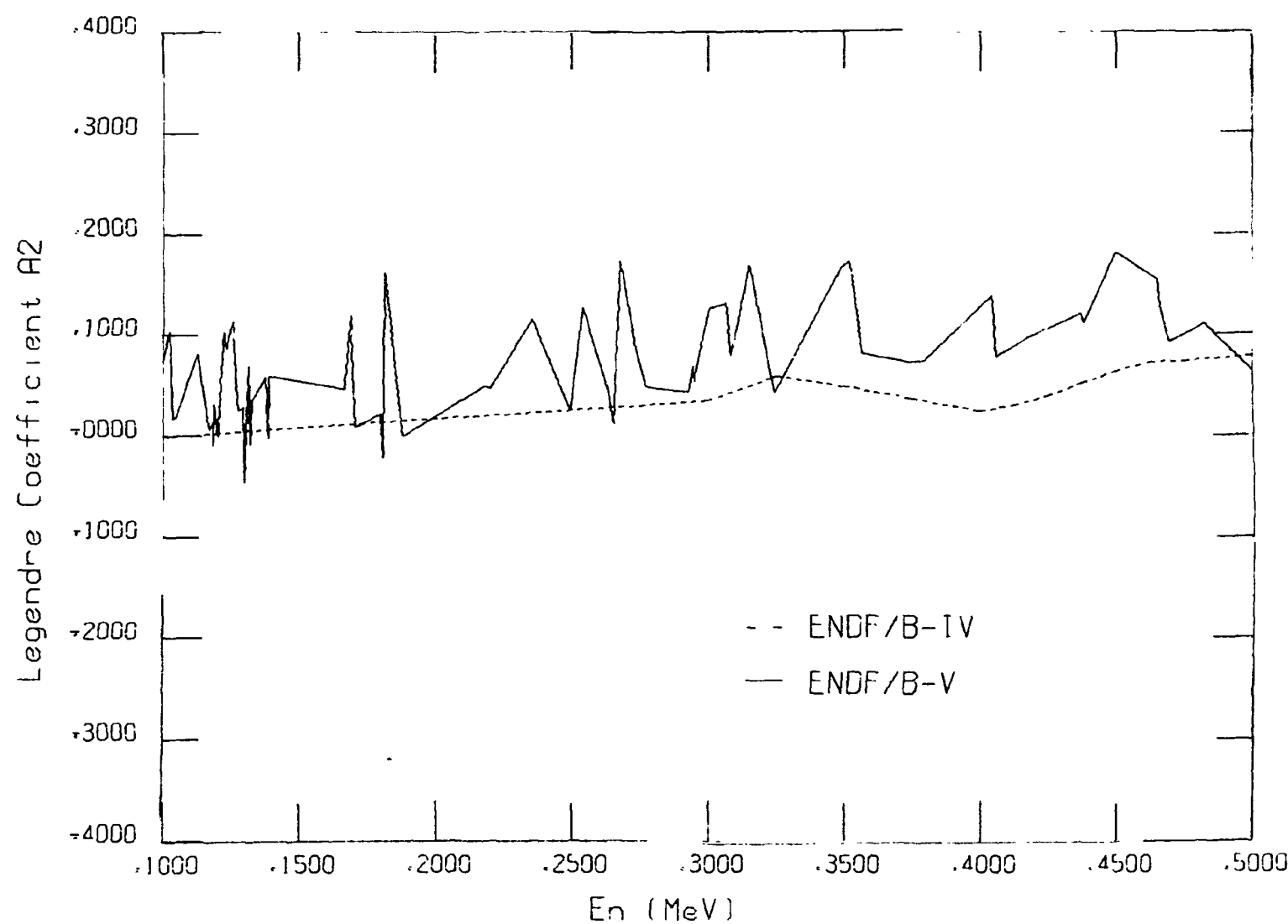
Fig. 23. Comparison of ENDF/B-V A2 Legendre coefficients for the angular distributions of elastically scattered neutrons with ENDF/B-IV from 100 keV to 500 keV.
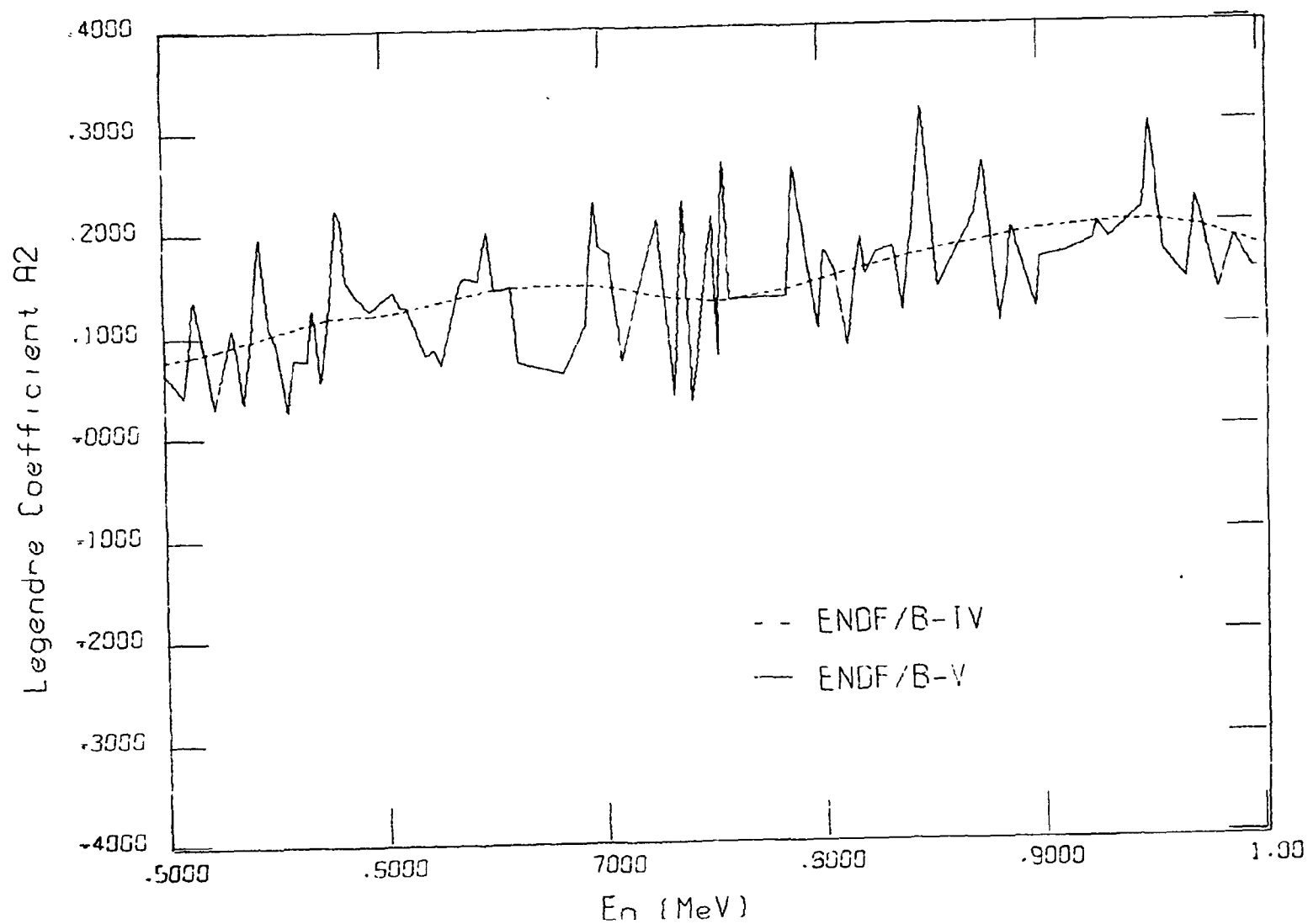
Fig. 24. Comparison of ENDF/B-V A2 Legendre coefficients for the angular distributions of elastically scattered neutrons with ENDF/B-IV from 500 keV to 1 MeV.

Fig. 25.   Comparison of ENDF/B-V A2 Legendre coefficients for the angular distributions of elastically scattered neutrons with ENDF/B-IV from 1 MeV to 2.2 MeV.